AD_____

Award Number: **W81XWH-08-2-0004**

TITLE: **"Targeted Delivery of Carbon Nanotubes to Cancer Cells"**

PRINCIPAL INVESTIGATOR: **Ellen Vitetta, PhD**

CONTRACTING ORGANIZATION: **University of Texas Southwestern Medical Center at Dallas**
Dallas, Texas 75390

REPORT DATE: **September 2009**

TYPE OF REPORT: **FINAL**

PREPARED FOR: U.S. Army Medical Research and Materiel Command
Fort Detrick, Maryland 21702-5012

DISTRIBUTION STATEMENT:

x Approved for public release; distribution unlimited

REPORT DOCUMENTATION PAGE

Form Approved
OMB No. 0704-0188

1. REPORT DATE *09/01/2009*	**2. REPORT TYPE** FINAL	**3. DATES COVERED** *(From - To)* 14 Dec 2007–31 Aug 2009

4. TITLE AND SUBTITLE

"Targeted Delivery of Carbon Nanotubes to Cancer Cells"

5a. CONTRACT NUMBER

5b. GRANT NUMBER W81XWH-08-2-0004

5c. PROGRAM ELEMENT NUMBER

6. AUTHOR(S)
Vitetta, Ellen S., Marches, Radu., Draper, Rockford

5d. PROJECT NUMBER

5e. TASK NUMBER

5f. WORK UNIT NUMBER

7. PERFORMING ORGANIZATION NAME(S) AND ADDRESS(ES)

University of Texas Southwestern Medical Center at Dallas
Dallas, TX 75390-8576

8. PERFORMING ORGANIZATION REPORT NUMBER

9. SPONSORING / MONITORING AGENCY NAME(S) AND ADDRESS(ES)
U.S. Army Medical Research
And Material Command
Fort Detrick, Maryland
21702-5012

10. SPONSOR/MONITOR'S ACRONYM(S)

11. SPONSOR/MONITOR'S REPORT NUMBER(S)

12. DISTRIBUTION / AVAILABILITY STATEMENT

Approved for public release; distribution unlimited

13. SUPPLEMENTARY NOTES

14. ABSTRACT

The current antitumor strategies, including chemotherapy, radiotherapy, naked and/or conjugated monoclonal antibody (MAb) therapy or combinations of these have major limitations ranging from insufficient cytotoxicity to severe side effects. A potential solution is the use of targeted nanoparticles such as carbon nanotubes (CNTs). CNTs have been demonstrated to possess unique properties including the ability to emit heat when exposed to either near-infrared (NIR) light. The proposal test the possibility to use targeted CNTs to selectively ablate tumors by the local heat generated by cell-bound CNTs under NIR light exposure. The present study describes the preparation of conjugates with MAbs indirectly or directly coupled to CNTs and the characterization of the chemical and biological properties of the resulting MAb-CNT conjugates. We, thus, prepared MAb-CNT conjugates with stable chemical structure. The CNTs preserved the key spectral properties, are not toxic and are stable in physiological buffers. They show a high tumor cell specificity and selective thermal depletion of tumor cells in cultures or in mouse models. This study will test the hypothesis that chemically stable nanoparticles, such as CNTs, might represent an alternative strategy to the current antitumor agents and provide a proof-of-principle for the therapy of at least a number of skin tumors.

15. SUBJECT TERMS
Carbon nanotubes, tumor targeting, monoclonal antibody

16. SECURITY CLASSIFICATION OF:			**17. LIMITATION OF ABSTRACT**	**18. NUMBER OF PAGES**	**19a. NAME OF RESPONSIBLE PERSON USAMRMC**
a. REPORT U	**b. ABSTRACT** U	**c. THIS PAGE** U	UU	36	**19b. TELEPHONE NUMBER** *(include area code)*

Standard Form 298 (Rev. 8-98)
Prescribed by ANSI Std. Z39.18

Table of Contents

INTRODUCTION

The objective of this project is to target carbon nanotubes (CNTs) to tumor cells and thermally ablate the cells by exploiting the ability of CNTs to absorb energy in regions of the electromagnetic spectrum that penetrate tissue and convert the energy to heat.

BODY

Task 1. To attach MAb to CNTs.

I. Non-Covalent Attachment of MAbs to CNTs Adsorbed with Biotinylated Fatty Acid Conjugates
This is a 2-step procedure that involves CNTs dispersion with biotinylated polar lipids, preparation of neutravidin-derivatized targeting MAb followed by their coupling.

CNT Dispersion by Biotinylated Polar Lipids**.** Single-walled CNTs (HiPco) were dispersed in 166 μM 1, 2-distearoyl-sn-glycero-3-phosphoethanolamine-N-[biotinyl(polyethylene glycol) 2000] (DSPE-PEG(2000)-biotin) by sonication. DSPE-PEG-biotin excess was removed by two times centrifugation for 15 min at 90,000 *x g*. The pellet was resuspended in 1 ml of DI water. The samples were then centrifuged two times for 10 min at 16,000 *x g* at room temperature and the upper 50% of the supernatant containing the biotinylated CNTs (B-CNTs) was recovered.

The resulting B-CNT suspension contained 0.06 mg CNT/ml and ≤ 3 parts per million metals, as determined by thermal gravimetric analysis (TGA). The dispersions were stable and did not aggregate at room temperature for over 120 days. Atomic force microscopy (AFM) analysis demonstrated that the suspension was homogenous the CNTs were either individually dispersed or in small bundles. The lengths of the CNTs ranged from 0.2 to 1.4 μm with an average of 0.59 μm (**Fig. 1a**). Analysis by transmission electron microscopy (TEM) of the B-CNT samples probed with gold-labeled goat anti-biotin demonstrated that biotin was distributed along the entire surface of the B-CNT (**Fig. 1b**). The biotin content of the B-CNT dispersion was determined by competitive enzyme-linked immunosorbent assay (ELISA). This was accomplished by adding dilutions of the B-CNT dispersion to biotin-horseradish peroxidase (HRP) and plating them onto neutravidin (NA)-coated plates. The amount of HRP-labeled biotin was detected by the development of color in the presence of the 2, 2'-azino-bis(3-ethylbenzothiazoline-6-sulfonic acid) (ABTS) substrate. Using this assay, we found that the content of biotin was 0.02 mmol per gram of B-CNT. The UV-Vis-NIR spectra of the B-CNTs confirmed the quality of these dispersions with the presence of electronic transitions between van Hove singularities suggesting that the optical properties of the CNTs were maintained following the adsorption of DSPE-PEG-biotin (**Fig. 1c**). The Raman spectra of the B-CNTs showed a number of well characterized CNT resonances such as the tangential (G-band) peak at 1590 cm^{-1}, confirming the presence of CNTs in the sample (**Fig. 1d**).

Preparation of MAb-NA Conjugates**.** To couple the B-CNTs to MAbs, we used a modified protocol. Briefly, 10 mg of IgG anti-CD22 (RFB4) or anti-CD25 (RFT5) in 1 ml of 0.15 M borate buffer, 0.1 mM EDTA, pH 8.5 were thiolated by incubation for 1 h at room temperature with a 20:1 molar excess of Traut's reagent. After incubation, the reaction was quenched with 0.1 M glycine. In parallel, 10 mg of NA dissolved in 1 ml of 0.01 M PBS, 0.1 mM EDTA, pH 7.4, were activated by 30 min incubation at room temperature using a 6:1 molar excess of MBS.

The unreacted Traut's reagent and MBS were removed by gel-filtration on Sephadex G-25 columns in 0.01 M PBS, 0.1 mM EDTA, pH 7.4. The thiolated MAb was conjugated to the activated NA at a molar ratio of 1:2 for 2 h at room temperature with gentle shaking. The resultant conjugate was purified by gel-filtration on a Sephacryl S-300 HR column (GE Healthcare) using 0.1 M PBS, 0.05% Tween-20, pH 7.4 (**Fig. 2a**). The protein concentration in the purified conjugate was quantified using the bicinchoninic acid (BCA) protein assay (Pierce Endogen). The size and

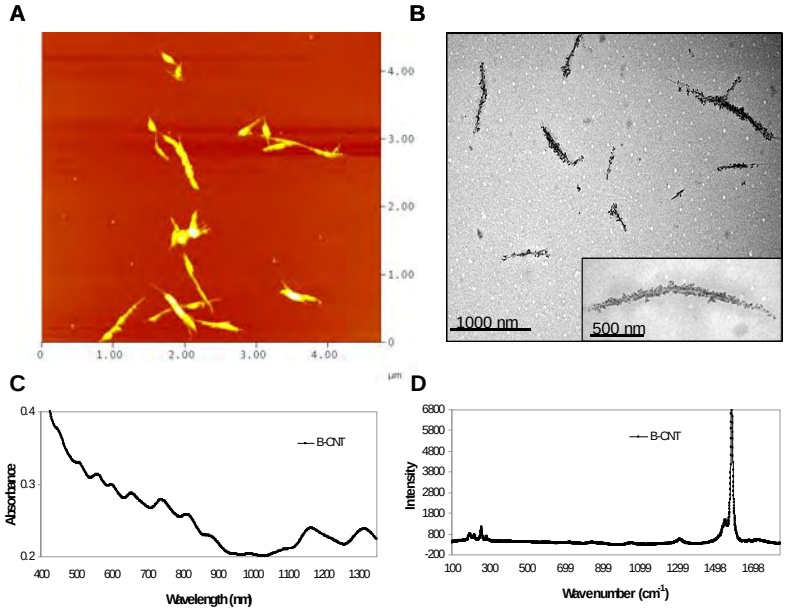

Figure 1. Analysis of the dispersed CNTs. The CNTs were dispersed by sonication in the presence of DSPE-PEG-biotin then washed/centrifuged twice at 90,000*xg* and twice at 16,000*xg*. The last supernatant that contains the dispersed CNTs was collected. **A.** Atomic force microscopy (AFM) indicates a good dispersion of the CNTs. **B.** TEM images of B-CNTs show uniform distribution of biotin after immunodetection with gold-labeled anti-biotin. **C.** UV/Vis spectra of CNT dispersions show multiple well-defined peaks compared to the spectra of the initial bundled CNTs. **D.** Raman spectra indicates a strong G band signature (1590 cm^{-1}), a diagnostic for CNTs, and a very low D band signal (1350 cm^{-1}), indicative of amorphic carbon structures.

integrity of the conjugate was analyzed by western blot. The samples were electrophoresed on a 7.5% non-denaturing polyacrylamide gel and transferred to polyvinylidene difluoride membranes (Bio-Rad Laboratories, Hercules, CA), probed with HRP-labeled sheep anti-mouse IgG, and visualized using an enhanced chemiluminescence system (GE Healthcare) (**Fig. 2b**).

To determine whether B-CNTs were inherently cytotoxic (in the absence of NIR), cells from the IgM^+ $CD22^+CD25^-$ Burkitt's lymphoma cell line Daudi, were incubated for 24 h with up to the highest amount of B-CNTs used in the binding and killing assays (3.6 μg). No toxicity was observed using a [^{3}H]-Thymidine incorporation assay (data not shown).

Preparation, purification, and analysis of noncovalent MAb-CNT complexes. Fresh MAb-CNTs were prepared immediately before use by mixing B-CNT with MAb-NA in a 1:2 (w/w) ratio. The mixture was placed on a rocker for 35 min at room temperature and vortexed gently every 5 min. After coupling, the mixture was centrifuged for 5 min at 16,000 *x g* at 4°C, the supernatant containing unreacted MAb-NA was discarded, and the pellet was resuspended in 40 μl of PBS for every 3.6 μg B-CNT and used immediately.

II. Covalent Attachment of MAbs to carboxyl-functionalized CNTs

In this approach we used carboxyl-functionalized CNTs to which we covalently coupled targeting MAbs. Carboxyl-functionalized CNTs (0.5 mg) were dispersed in 1 ml of 0.1 M 2-[*N*-morpholino]ethane sulfonic acid (MES) buffer, pH 4.5 with 0.2% Tween-20 (activation buffer) by sonication with a 2 mm probe tip connected to a Branson Sonifier 250 (VWR, West Chester, PA) for 5 min at a power level of 10 W, with the sample immersed in ice. The mixture was then centrifuged at 16,000 x *g* for 15 min to remove undispersed material. The supernatant containing the dispersed CNTs was recovered. The carboxyl groups on the CNTs were activated by incubation for 30 min at room temperature with 2 mM EDC and 5 mM NHS. The excess reagents were removed by centrifugation in Amicon Ultra-4 centrifugal filter unit (Millipore, MA) and rinsed with binding buffer (0.1 M PBS, pH 7.2 with 0.2% Tween-20). The activated CNTs were recovered in 1 ml binding buffer and reacted with 10 mg IgG anti-CD22 (RFB4) or IgG anti-CD25 (RFT5) MAbs for 2 h at room temperature by gentle rocking. The control for covalent coupling was a mixture of MAbs and non-activated, carboxyl-functionalized CNTs. The unreacted MAbs were removed by centrifugation at 16,000 x *g* for 30 min. The supernatant containing unreacted MAb was discarded, and the pellet was resuspended and washed twice in 1 ml of phosphate buffered saline (PBS) buffer (10 mM, pH 7.4). After each wash, the CNTs were briefly sonicated for 10 seconds at a power level of 10 W. The amount of CNT-bound MAbs was quantified using the bicinchoninic acid (BCA) protein assay (Pierce Endogen) and the CNT concentration was determined by the absorbance at 808 nm using a DU-730 Beckman-Coulter UV/Vis spectrophotometer (Fullerton, CA). In order to directly visualize the binding of MAb-CNTs to target cells, CNTs were conjugated to both MAb and enhanced green fluorescent protein (EGFP). For the coupling reaction 10 mg MAb and 100 μg EGFP were reacted with activated CNTs as mentioned above.

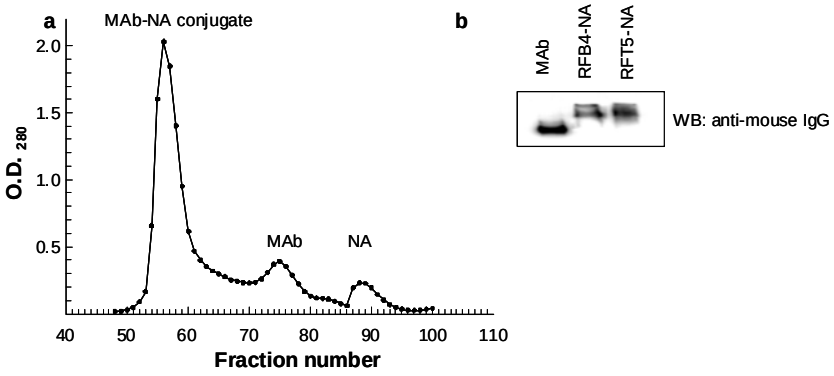

Figure 2. Analysis of MAb-NA conjugates. *(a)* A typical chromatographic separation of RFB4-NA from unconjugated RFB4 and NA using a Sephacryl S-300 HR column. Fractions of the first peak containing the RFB4-NA conjugate were pooled and concentrated. *Inset:* Purified RFB4-NA, RFT5-NA or MAb were electrophoresed under non-denaturing conditions on a 7.5% polyacrylamide gel and immunoblotted with HRP-labeled sheep anti-mouse IgG. Data in *a* and *b* are representative of at least three independent experiments.

Relationship to the work of others: The first critical challenge in the field of targeted CNTs is to create soluble and stable CNTs that retain both the specificity of the targeting moiety and the thermal activity of the CNTs even in

serum at physiological temperatures. Our strategies involved noncovalent attachment of targeting moiety consisting of MAb-NAs to the dispersed biotinylated CNTs (non-covalent MAb-CNTs) and chemical link of the targeting MAb to carboxyl-functionalized CNTs (covalent MAb-CNTs). The first approach gave us the flexibility to "assemble" the targeted CNTs using any tumor-binding MAb. Also, the strategy of generating dispersed CNTs using biotinylated polar lipids has the advantage of preventing subsequent chemical treatments that remove the adsorbed polar lipids and/or destroy the optical properties of CNTs. Of equal importance is the specificity of the targeting strategy. Thus, previous studies have demonstrated that folic acid -coated CNTs could be targeted to folate receptor (FR)-positive cells and that NIR light killed the cells (1). Although FR-negative cells were used as a control, CNTs coated with an irrelevant control peptide or ligand were not. Another published approach for targeting CNTs to cells was to attach MAbs by direct adsorption that can be used in photothermal therapy (2) or imaging (3). However, attachment of MAbs by direct adsorption on CNTs involves a potential loss of the targeting function of the MAbs and indeed in the study cited, specificity controls were not reported, and cell viability studies showed 50% collateral damage by the irrelevant MAb-CNT control following exposure to NIR light (2).

The potential cytotoxicity of CNTs has been of concern for their use for therapy. One of the major challenges is to minimize their nonspecific interaction with serum proteins and/or cells and tissues and increase their half-life in the circulation. In previous reports, this was achieved by coating CNTs with biocompatible compounds, such as hydrophilic uncharged polymers including poly-(ethylene glycol) (PEG). Pharmacokinetics studies with such coated CNTs have demonstrated that CNTs dispersed by different noncovalent procedures are not toxic to mice (4-6).

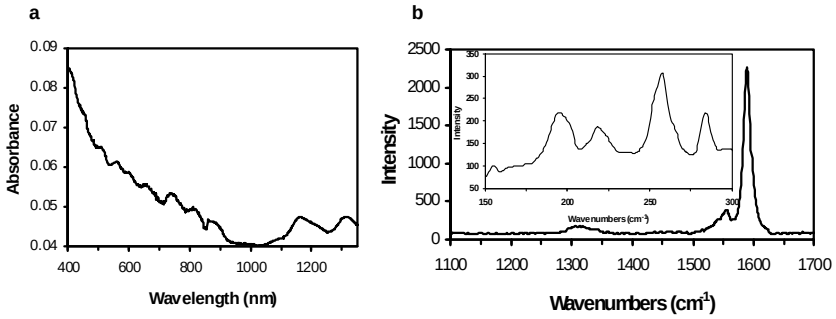

Figure 3. Optical properties of CNTs following coupling with MAbs. *(a)* UV-Vis-NIR spectra of RFB4-CNTs show the same metallic and semi-conducting CNT types as observed for the B-CNTs, indicating the retention of the optical properties of CNTs following the coupling with RFB4-NA. *(b)* Raman spectra of RFB4-CNTs show an intense G band (~1590 cm^{-1}) as the B-CNTs, indicating the presence of CNTs in the conjugate. The spectra are representative of three independent experiments.

Moreover, carboxyl functionalization, as we used in our second approach, increases their solubility and decreases their cytotoxicity (7). In our study, the viability of cells cultured with non-binding MAb-CNTs was indistinguishable from that of cells grown in the absence of CNTs.

Task 2. **<u>To purify the MAb-CNT constructs thus removing unconjugated NA-MAb or biotinylated intermediates that might interfere with subsequent targeting studies. The physical-chemical properties of the MAb-CNTs will also be characterized to determine particle size using TEM and atomic force microscopy (AFM).</u>**

I. **Analysis of noncovalent MAb-CNT conjugates.**

The UV-Vis-NIR spectra of the MAb-CNT conjugates displayed the same metallic and semi-conducting CNT types as observed for the B-CNTs, indicating that the optical properties of the CNTs were not affected by the coupling (**Fig. 3a**), and the characteristic CNT resonances displayed in the Raman spectra of the MAb-CNTs again confirmed the presence of CNTs in the sample (**Fig**. **3b**).

II. **Analysis of covalent MAb-CNT conjugates.**

For AFM analysis, the samples were transferred into deionized water. The dimensions of dispersed MAb-CNTs were determined using AFM. **Figure 4a** shows a representative image of the CNTs after attaching them to RFB4. The dried MAb-CNT sample showed signs of cross-linking with lengths that ranged from 0.5 – 2.0 μm with an average length of 1.0 ± 0.3 μm (number of measurements, n = 19). The lengths of the carboxylated-CNTs ranged from 0.2 – 1.5 μm with an average length of 0.7 ± 0.3 μm (n = 31) (data not shown). The diameters of the MAb-CNTs ranged from 9.0 – 20.0 nm with an average diameter of 12.3 ± 2.5 nm (n = 20). The diameters of the carboxylated-CNTs ranged from 2.8 – 9.0 nm with an average diameter of 5.9 ± 1.8 nm (n = 20), indicating a surface coating of the Tween 20 surfactant. Comparing the diameters of the carboxylated-CNTs with those of the RFB4-coupled CNTs suggests that the average 6nM increase in diameter can be attributed to the presence of the MAb. The AFM images confirm the formation of the RFB4-CNT conjugate, although the nature of the linkage could be covalent and/or non-covalent. In order to confirm that the linkage was covalent, the MAb-CNTs were dispersed in sodium dodecylsulfate (SDS) and electrophoresed on a 7.5% polycrylamide gel electrophoresis (PAGE) under nonreducing conditions. The control sample contained a mixture of equivalent amounts of CNTs and MAb. As shown in **Fig. 4b**, no IgG was detected in the RFB4-CNT samples, demonstrating that the CNT-bound IgG remained in the loading well attached to CNTs. In contrast, a MAb band was detected in the "mixture" control. Taken together, these data indicate that the linkage between the MAbs and the CNTs was covalent. We next determined if the optical properties and structure of the CNTs were affected by the covalent coupling. Pertinent to their use in photothermal therapy, the UV-Vis-NIR spectrum indicated that CNTs preserve their absorption in the NIR region **(Fig. 4c).** The resonant Raman scattering analysis indicates the quality of CNTs in the conjugate (**Fig. 4d**). Indeed, the RFB4-CNT conjugate exhibited the characteristic G band at ~1590 cm^{-1} derived from graphitic carbons. The high intensity of the G-band, assigned to the tangential mode of the graphene sheet, compared with the D-band (~1370 cm^{-1}), ascribed to the Raman mode of the amorphous carbon, indicated the high purity of the sample.

Relationship to the work of others: The use of biotinylated phospholipids to non-covalently coat and disperse CNTs has the advantage of not disrupting the electronic structure of the CNTs. However, there is a potential limiting factor in using these CNTs in animals because non-covalently attached lipid material might be displaced by other macromolecules in biological fluids, resulting in the removal of the targeting moiety (4). The chemical and binding stability of the MAb-CNT conjugates as well as their stability in serum are important to establish before using them *in vivo*. For this reason, we tested an alternative strategy where the targeting molecule was covalently coupled to the CNTs. In order to do this, we used the carboxylic acid groups on chemically oxidized CNTs, which have the advantage of well-described chemistry (8-11). A potential disadvantage is that covalent modification of CNTs may interfere with the electronic and optical properties of the CNTs. However, previous reports (12) indicated that water-soluble, mildly carboxylic acid-modified CNTs obtained by oxidative pretreatments retain their van Hove singularities which are critical for the absorption of NIR light. Previous reports have demonstrated that an anti-CD20 MAb covalently coupled to CNTs retained both linkage stability and specific targeting (13). These conjugates were used to deliver radionuclides to tumor cells *in vivo* and not for their ability to convert NIR light to heat, Since the chemistry of MAb attachment involved a sidewall ylide cycloaddition followed by 2-(4-isothiocyanatobenzyl)-1, 4,7,10-tetraazacyclododecane-1,4,7,10-tetraacetic (DOTA) and succiminidyl-4-(N-maleimidomethyl)cyclohexane-1-carboxy-(6-amidocaproate rather than direct attachment to terminal carboxyl groups, the photothermal property of the CNTs might have been compromised. Indeed, one of the major concerns with the covalent attachment of targeting ligands is that chemical stability can increase at the expense of photothermal efficacy due to the defects in the sp^2 hybridization of the CNTs induced by chemical functionalization. It has been noted that the Raman profile and NIR absorption of CNTs are significantly affected by their covalent modification (14). However, we found that chemical coupling of the MAb to CNT did not destroy the optical properties critical for the conversion of NIR light into heat.

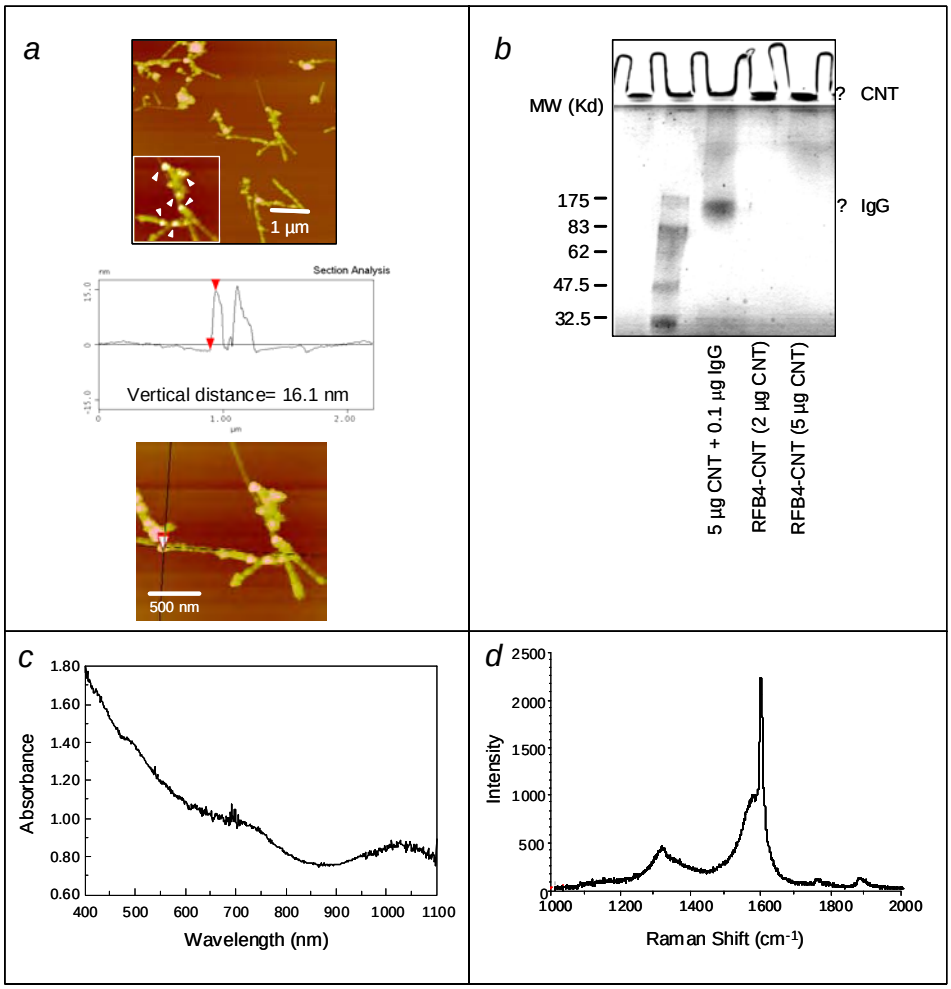

Figure 4. Physical and optical properties of RFB4-CNTs. *(a)* AFM image indicating the attachment of MAbs to CNTs. The enlarged inset shows where the MAbs are attached to the CNTs (arrowheads). The diameter of a coated region (~16 nm) is determined by AFM height analysis (*bottom panel*). This AFM image is representative of AFM images acquired from two unique MAb-CNT dispersions. *(b)* Stability of RFB4-CNTs. Purified RFB4-CNTs or a mixture of carboxylated CNTs and RFB4 (control) were subjected to SDS-PAGE. Samples containing 3 or 5 µg CNTs were loaded on the gel. The stacking gel shows the accumulation of CNTs whereas dissociated IgG migrated into the gel. The presence of dissociated protein was detected by staining with SimplyBlue SafeStain. *(c)* UV-Vis-NIR spectrum of RFB4-CNTs. *(d)* Raman spectrum of the carboxylated CNTs after covalent coupling of MAb. G band at ~1590 cm^{-1} is the characteristic Raman signal for CNTs. One representative experiment of three is shown in each panel.

Task 3. **<u>To test targeting of MAb-CNTs to cells *in vitro*.</u>**

I. **Specific binding of noncovalent MAb-CNT conjugates.**

The ability of the MAb-CNT conjugates to bind to antigen-positive but not antigen- negative target cells was assessed by flow cytometry. The components of the cell-bound MAb-CNT were detected using fluorescein-isothiocyanate-labeled goat anti-mouse Ig (FITC-GAMIg) (which reacts with mouse MAb) and phycoerythrin-labeled streptavidin (PE-SA) (which reacts with biotin), respectively. We found that RFB4-CNT and RFB4 (positive control) bound equally well to Daudi cells whereas RFT5-CNT (negative control) bound poorly ($p < 0.001$) (**Fig. 5a**). Conversely, RFT5-CNT and RFT5 bound equally well to $CD22^{-}CD25^{+}$ phytohemagglutinin (PHA)-

activated peripheral blood mononuclear cells (PBMCs) (95% $CD25^+$ cells), whereas the negative control conjugate, RFB4-CNT, did not ($p < 0.002$) (**Fig. 5b).** These results demonstrate that the coupling of the MAbs to CNTs does not alter their MAb-binding activity and that the MAb-CNTs bind to antigen- expressing cells as specifically as the uncoupled MAbs.

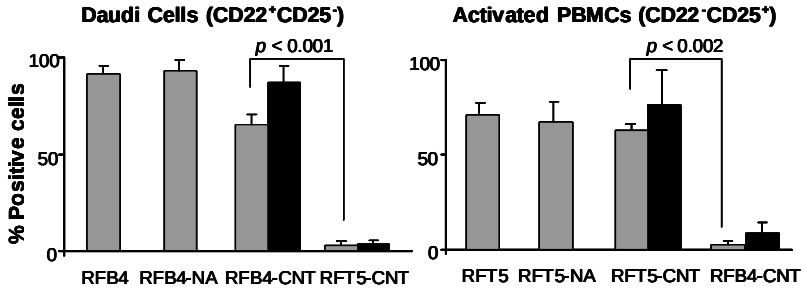

Figure 5. Binding of MAb-CNTs to target cells. The specific binding of RFB4-CNT to Daudi cells using RFT5-CNT as a negative control and the specific binding of RFT5-CNT to activated PBMCs (>95% T cells) using RFB4-CNT as negative control. A million cells were incubated with saturating concentrations of RFB4-CNT or RFT5-CNT and then incubated with either FITC-GAMIg to detect the MAb moiety or with PE-SA to detect the B-CNT moiety and analyzed by flow-cytometry.

II. **Specific binding of the covalent MAb-CNT conjugates.**

We determined the ability of these MAb-CNT conjugates to bind to $antigen^+$ but not $antigen^-$ target cells using flow cytometry. The cell-bound MAb-CNTs were detected using FITC-GAMIg. We found that RFB4-CNTs bound well to Daudi cells whereas the RFT5-CNTs (negative control) bound poorly (**Fig. 6a and b)**. Conversely, RFT5-CNTs and RFT5 bound equally well to $CD22^-CD25^+$ PHA-activated PBMCs (95% $CD25^+$ cells), whereas the negative control conjugate, RFB4-CNT, did not **(Fig. 6a and b)**. Additional experiments using non-activated, carboxyl-functionalized CNTs incubated with targeting antibody (control) indicated no detectable binding to cells (data not shown). This indicates that CNTs are free of adsorbed MAb. Taken together, these results demonstrate that the MAb-CNTs bind specifically to antigen- expressing cells. The binding to target cells was confirmed by flow cytometric analysis of the CNTs co-coupled to targeting MAb and EGFP **(Fig 6c, left panel)** and fluorescence microscopy (**Fig 6c, right panel).** The extensive binding and receptor cross-linking was confirmed by the massive homotypic adhesion of cells **(Fig 6c, right panel).**

The stability of the MAb-CNT conjugate was established by incubating RFB4-CNTs (1 μg CNTs) in 500 μl mouse serum at 37°C for up to 24 h. At the end of incubation, the RFB4-CNTs were recovered by centrifugation and then tested for their ability to bind to $CD22^+$ Daudi cells, using RFT5-CNT as negative control. As shown in **Figure 7**, we found that their binding was not diminished.

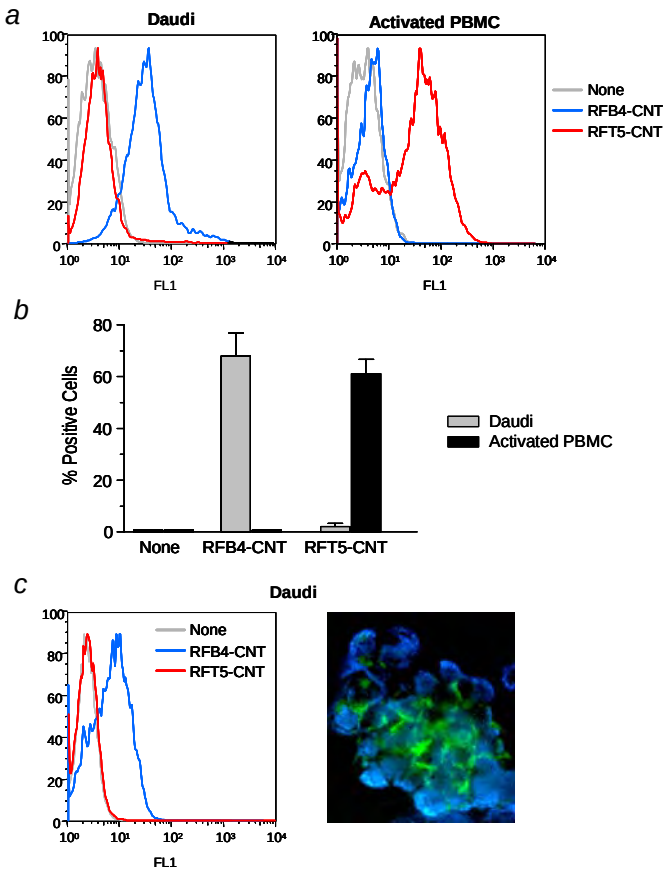

Figure 6. Specific binding of MAb-CNTs to target cells. *(a)* Daudi cells or PHA-activated human PBMCs were stained with either RFB4-CNTs or RFT5-CNTs (1 µg CNT) followed by FITC-GAMIg and cells were analyzed by flow cytometry. Histograms showing the staining with RFB4-CNTs (blue line) and RFT5-CNTs (red line) are overlaid on the ones corresponding to unstained cells (grey line) in each panel. *(b)* The results of three independent binding experiments are presented as means of % positive cells ± SD. The binding of MAb-CNTs to target *vs.* non-target cells was highly specific ($p<0.01$) *(c)* The binding of RFB4-CNTs to Daudi cells was confirmed by direct fluorescence using CNTs co-conjugated to RFB4 and EGFP. Cell binding was revealed by flow-cytometry *(left panel)* and fluorescence microscopy *(right panel)*.

Relationship to the work of others: The targeting of CNTs to tumor cells can be accomplished by coating them with cell-binding ligands such as peptides or MAbs (1-3,15,16). Several studies have reported that the targeting of such CNTs is "specific" (1-3,13,15,16) but no study has used both a control ligand and a control cell to convincingly demonstrate ligand-specific thermal ablation of tumor cells with CNTs. In our study we provided clear evidence of specific binding to target cells with both types of MAb-CNTs.

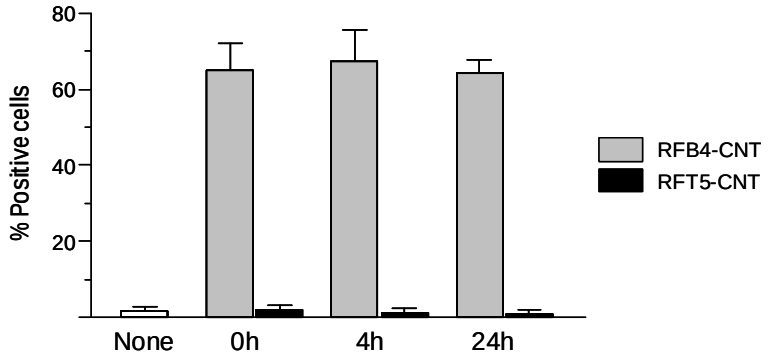

Figure 7. Binding stability of RFB4-CNTs. The stability of the RFB4-CNTs *in vitro* was determined by incubating them (1 μg CNT) in mouse serum at 37°C for 0, 4 and 24 h. At each time point, the RFB4-CNTs were recovered by centrifugation, washed with PBS and incubated with Daudi cells and the positive binding detected by flow-cytometry. Data represent mean ± S.D. of at least three independent experiments.

Task 4. <u>To assess the thermal ablation of the tumor cells in the model cell systems upon exposure to NIR light or RF waves.</u>

I. **Thermal ablation of target cells by noncovalent MAb-CNT conjugates upon exposure to NIR.**
Having demonstrated that the MAb-CNT conjugates retained the binding activity of the MAb and the optical properties of the CNTs, we next determined whether cells targeted by the MAb-CNTs could be thermally ablated following exposure to NIR light. Cells were incubated with the MAb-CNTs in PBS, washed 3 times with PBS and then dispensed into 96-well plates in cell culture media. The cells in the plate were exposed to an 808 nm laser (5 W/cm^2) for 7 min and pulsed for the next 12 h with 1 μCi [^{3}H]-Thymidine to assess cell viability. As shown in **Fig. 8a**, as compared to treatment with the non-binding RFT5-CNTs, the viability of the RFB4-CNT-treated Daudi cells was significantly reduced following exposure to NIR light ($p<0.0001$). Conversely, when activated PBMCs were used as target cells, RFT5-CNT, but not RFB4-CNT, killed the cells following exposure to NIR light ($p<0.0001$) (**Fig. 8b).** These experiments demonstrate that the binding of the MAb-CNTs to their respective antigen-positive target cells leads to their specific ablation following exposure to NIR light.

Thermal ablation of target cells by covalent MAb-CNT conjugates upon exposure to NIR.

We tested whether cells targeted by the covalent MAb-CNTs could be thermally ablated following exposure to NIR light. Cells were incubated with the MAb-CNTs in PBS and after the excess unbound CNTs were removed, cells were suspended in culture medium and dispensed into 96-well plates. The cells in the plate were exposed to an 808 nm laser (9.5 W/cm^2) for 4 min and pulsed for the next 12 h with 1 μCi [^{3}H]-Thymidine to assess their proliferative capacity, which is our standard method to measure cell viability. As compared to the non-binding control RFT5-CNTs, the viability of the RFB4-CNT-treated Daudi cells was significantly ($p<0.01$) reduced following exposure to NIR light **(Fig 9a**). Conversely, when activated PBMCs were used as target cells, RFT5-CNTs, but not the control RFB4-CNTs, killed the cells following exposure to NIR light **(Fig. 9b).** The selective photothermal damage responsible for the inhibition of proliferation was confirmed under light microscopy as the loss of morphological integrity in Daudi cells pretreated with RFB4-CNT (**Fig. 10b**) but not in untreated or control treated cells **(Fig. 10a and c).** The proliferation of cells treated with MAb-CNTs in the absence of NIR was significantly lower ($p<0.05$) than the proliferation of untreated cells **(Fig 9a and b)**. This may be due to an extensive cross-linking of the target antigen by the CNT-bound MAbs and subsequent signaling of growth arrest and/or apoptosis. This possibility is supported by the observation that cells undergo massive clustering. Indeed, Daudi cells pretreated with RFB4-CNTs formed "tissue-like" structure of aggregates with large contact areas after 12 h of incubation **(Fig. 10e)**. In contrast, no aggregates **(Fig. 10f)** and no inhibition of cell proliferation **(Fig. 9a)** occurred when cells were treated with control RFT5-CNTs. These indicate that the homotypic adhesion and the concurrent inhibitory effect are receptor-dependent and do not involve any CNT-mediated nonspecific adhesion. These experiments demonstrate that the binding of the MAb-CNTs to their target cells leads to their specific ablation following exposure to NIR light and the overall inhibitory effect is further enhanced by receptor hyper-crosslinking.

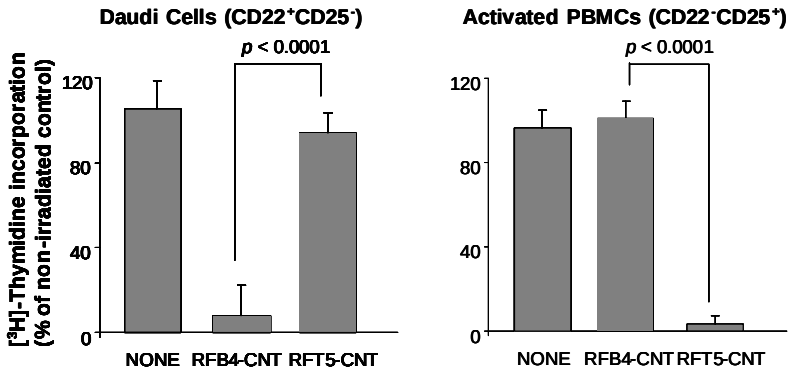

Figure 8. Ablation of MAB-CNT coated cells with NIR. The specific NIR-mediated thermal ablation of Daudi cells by RFB4-CNT using RFT5-CNT as negative control and of activated PBMCs (>95% T cells) by RFT5-CNT using RFB4-CNT as negative control. Cells (10^6) were incubated with saturating concentrations of RFB4-CNT or RFT5-CNT, wash out the excess and then dispensed into 96-well plates (10^5 cells/well). The cells were exposed for 7 min to 808 nm NIR light (5 W/cm^2), pulsed with 1μCi [^{3}H]-Thymidine and harvested 12 h later. The incorporated radioactivity was measured by liquid scintillation counting from triplicate samples. The percentage of radioactivity incorporated by each sample was calculated relative to corresponding non-irradiated sample. Data represent mean ± S.D. of at least three independent experiments. *P*-values were calculated utilizing paired, two-tail distribution Student's *t*-test.

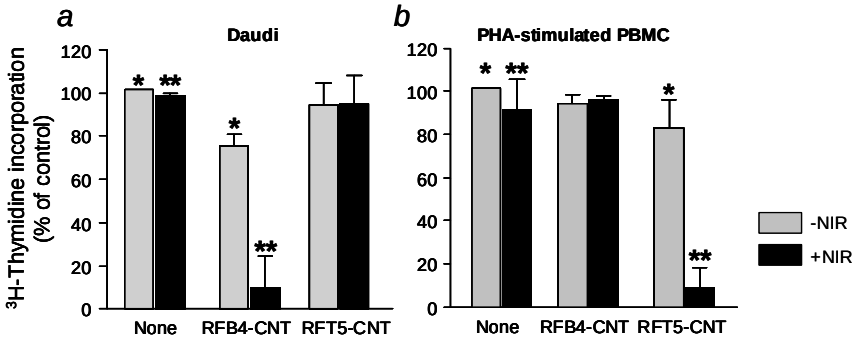

Figure 9. Specific killing of target cells by MAb-CNTs following exposure to NIR light. A million cells were incubated with MAb-CNTs containing 3 μg CNTs in PBS for 15 min at 4°C. Cells were washed three times with ice-cold PBS, and then 10^5 cells were dispensed in triplicate wells in a 96-well plate in 200 μl complete medium. The cells were exposed to continuous NIR light for 4 min at 9.5 W/cm^2. Cell death was assessed by pulsing the cells for the next 12 h with 1 μCi [^{3}H]-Thymidine/well and the incorporated radioactivity was measured by liquid scintillation counting. The incorporated radioactivity for each sample was calculated relative to the corresponding non-irradiated samples. *(a)* The specific killing of Daudi cells by RFB4-CNTs using RFT5-CNTs as the negative control. *(b)* The specific killing of activated PBMCs (>95% T cells) by RFT5-CNTs using RFB4-CNTs as the negative control (*, $p < 0.01$; **, $p < 0.05$). Data represent mean ± S.D. of at least three independent experiments.

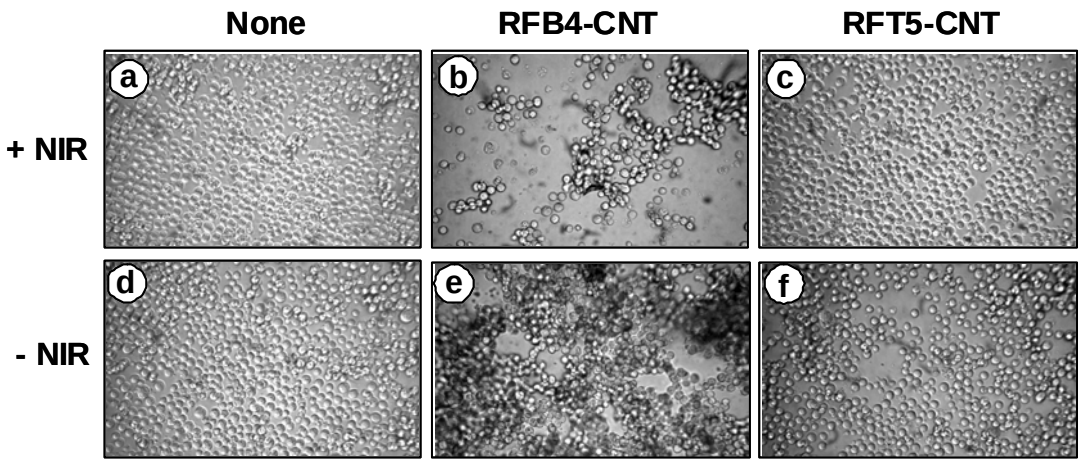

Figure 10. Morphological features of Daudi cells following treatment with MAb-CNTs and NIR irradiation. A million Daudi cells were incubated with or without MAb-CNTs containing 3 μg CNTs in PBS for 15 min at 4°C. Cells were washed three times with ice-cold PBS, and then $2x10^5$ cells were dispensed in a 24-well plate in 400 μl complete medium. The cells were exposed or not to continuous NIR light for 4 min at 9.5 W/cm^2. Cell morphology was assessed 12 h later by light microscopy (Magnification, x40 in all panels).

Relationship to the work of others: The use of NIR-resonant nanostructures, including gold nanoshells and CNTs, to thermally ablate cancer cells is being explored by several groups (1,2,17-20). The use of NIR light in the 700-1100 nm range for the induction of hyperthermia is particularly attractive because living tissues do not strongly absorb in this range (16). The critical aspect for selective CNT-mediated thermal ablation of cells is to stably attach targeting moieties that will not interfere with the optical properties of the CNTs and yet retain targeting specificity. We found that CNTs attached to MAbs by covalent bonds could thermally ablate target cells with the same efficiency as CNTs attached to MAbs by non-covalent bonds. CNT conjugates described in this study are biocompatible with cells *in vitro*. However, cells cultured with target-specific covalent MAb-CNTs did not proliferate as well due to receptor-mediated signaling of cell cycle arrest and/or cell death. This has been observed previously using cross-linking MAbs specific for different B cell surface markers and is therefore not surprising (21, 22).

Task 5. To determine the biodistribution and pharmacokinetics of MAb-CNTs in mice with and without tumors.

The final objective if this work is to determine the biodistribution and pharmacokinetics of these conjugates in mice. The model system is SCID mice bearing a s.c human B lymphoma. However, within the year allotted to this proposal there was insufficient time to finalize this task. A no-cost extension was therefore requested. The data from these studies will provide key information for the future design of local and systemic ablation of tumors in mice.

Quantification of noncovalent MAb-CNT conjugates in organ homogenates

As a preliminary step for determining the biodistribution of the CNTs, we set up a sensitive technique to determine the concentration of CNTs in homogenates of various mouse organs. We chose to use the intrinsic 1590 cm^{-1} Raman G-band signature of the CNTs to detect them. The homogenates were placed in glass-bottom dishes and measured by Raman spectroscopy. The G band peak area was integrated from 1570 cm^{-1} to 1620 cm^{-1} and averaged for multiple spectra and then plotted against the concentrations of CNTs. A typical Raman shift plot for serial dilutions of CNTs in PBS is shown in **Fig. 10a** and the standard curve in **Fig. 10b**. Similar standard curves were generated using homogenates of mouse organs spiked with CNTs. To this end mice were sacrificed and perfused with saline. Organs were collected, lyophilized and then mechanically homogenized after digestion with collagenase followed by the addition of sodium dodecyl sulfate (SDS). Then, known amounts of CNTs were added to the tissue

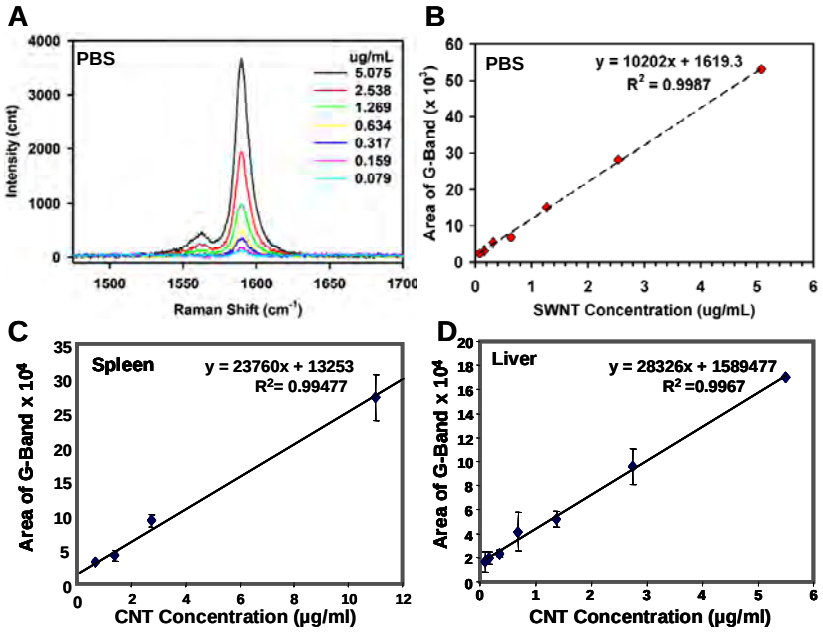

Figure 10. Standard Raman calibration curve of CNT solutions. *(a)* A typical Raman spectrum of CNT in PBS at different concentrations after subtracting background. *(b)* Standard curve for CNT concentration (G-band region intensity *vs.* CNT concentration) in PBS or *(c* and *d)* in lyophilized mouse liver and spleen tissue powder suspended in surfactant solutions.

homogenate. Two such standard curves generated for liver and spleen as shown in **Fig. 10c and d**. We were able to track the RFB4-CNTs in mice in different organs and at different time-points following injection. We found that the levels of the MAb-CNTs were the highest in the liver, where the levels did not fall following 60 hrs p.i. We detected the MAb-CNTs in the spleen and lung, where the levels remained steady for 60 hrs p.i. Levels of the RFB4-CNT were almost undetectable in the kidney as shown in **Fig. 11**.

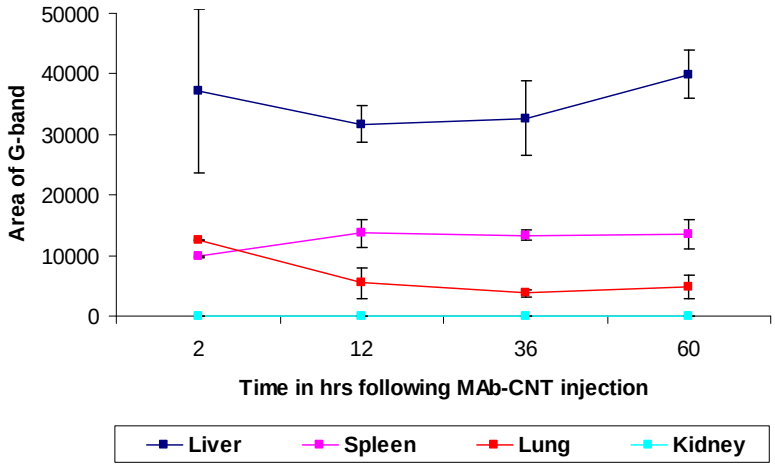

Figure 11. Organ distribution of RFB4-CNTs in mice as detected by the area under the G-band curve. Normal mice were injected i.v. with noncovalent MAb-CNTs. The animals were sacrificed at different time-points after injection and their organs harvested, lyophilized and suspended in surfactant solutions. The levels of CNTs in the organs at different time-points were determined by Raman spectroscopy after subtracting the background. The amplitude of the G-band was directly proportional with the level of CNTs.

Quantification of covalent MAb-CNTs in organ homogenates

We found that MAb-CNT conjugates generated with carboxylated CNTs had a very weak G-band Raman signal compared to non-carboxylated CNTs used for the preparation of non-covalent MAb-CNT conjugates. To improve the sensitivity of detection of one covalent MAb-CNTs, we captured the MAb-CNTs and then detect the MAb-CNTs with a radiolabeled antibody specific for the targeting MAb. In brief, we suspended mouse organs in SDS, sonicated them, and then prepared dilutions of covalent RFB4-CNTs. We then incubated the RFB4-CNTs with sheep anti-mouse coated magnetic beads (Dynabeads™). After removing the unbound material, we incubated the beads with ^{125}I-anti-RFB4 idiotype. Following the incubation, the beads were washed thoroughly and the radioactivity was measured in a gamma counter. As shown in **Fig. 12b**, we detected very low levels of MAb-CNT as compared with the amounts detected by Raman spectroscopy (**Fig 12a**). We also plan to develop an alternative

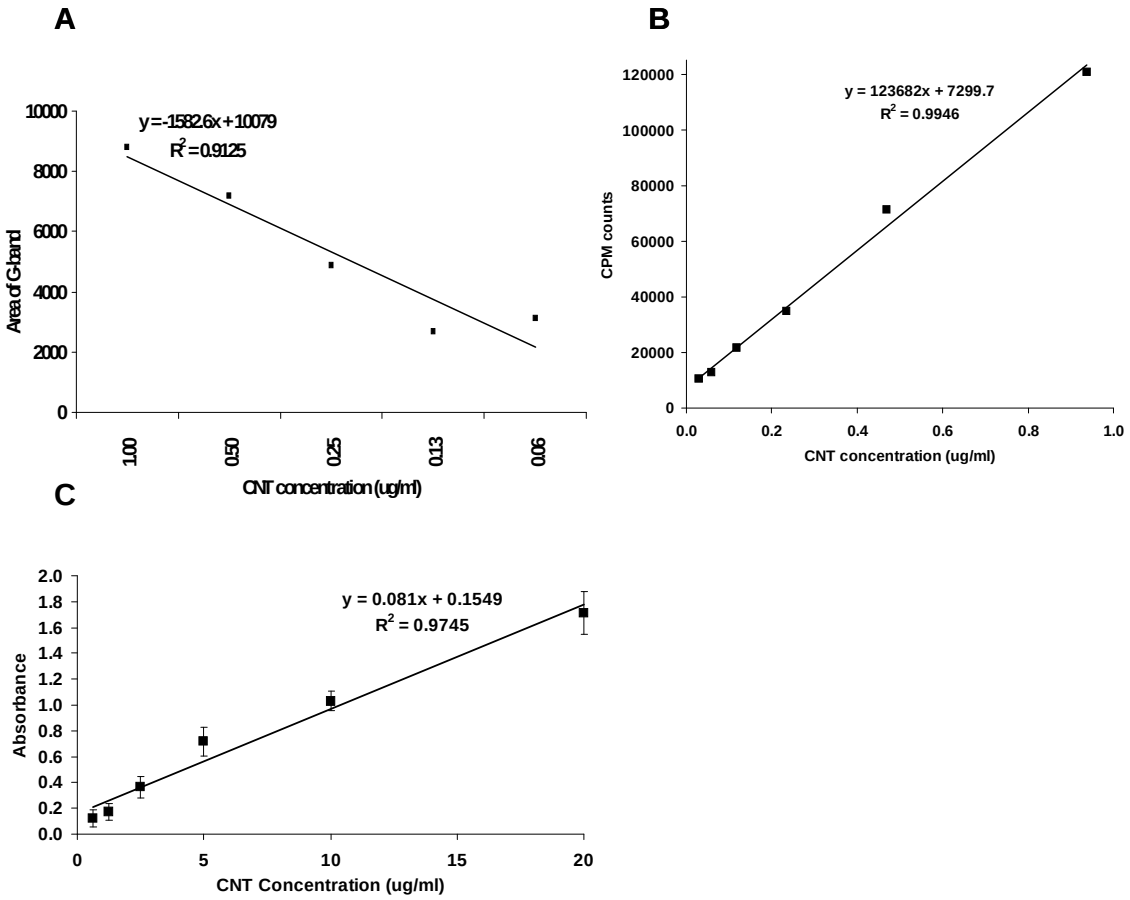

Figure 12. Standard calibration curves for covalent MAb-CNTs in liver homogenates and PBS. *(a)* Standard curve for MAb-CNTs in mouse liver homogenate using Raman spectroscopy. The curve was generated by plotting the area under the G-band curve against CNT concentration. *(b)* Standard curve for MAb-CNT in mouse liver homogenate using radioimmunoassay. Known concentrations of RFB4-CNTs dispersed in mouse liver homogenates were captured with sheep-anti-mouse-Ig-coated magnetic beads. The bound RFB4-CNTs were detected using ^{125}I-anti-RFB4 and measured in a gamma counter. The curve was generated by plotting the bound cpm counts *vs.* CNT concentration. *(c)* Standard curve for rabbit-Ig-CNT in PBS using ELISA. ELISA plates were coated with mouse anti-fullerene IgG. Rabbit IgG covalently coupled to CNT was added to the plate at different dilutions. After removing the unbound material, the plate was incubated with horseradish peroxidase-labeled goat anti-rabbit-Ig, washed, and the tetramethylbenzidine substrate was added. The color intensity was measured in an ELISA reader at 450 nm. The curve was generated by plotting the A_{450} *vs.* CNT concentration

method that should allow us to directly quantify CNTs. We found reports where a MAb had been generated against fullerenes that crossreacts with CNTs and can be used as an immunodetection agent in an ELISA assay (23,24). We coated ELISA plates with this MAb (10 ug/ml) and then incubated the plate with increasing concentrations of MAb-CNT. After removing the unbound material, we incubated the plate with goat anti-rabbit IgG coupled to horseradish peroxidase. Detection was done in the presence of tetramethylbenzidine substrate and then read the absorbance at 450 nm (**Fig. 12c).** Despite the cross-reactivity of the anti-fullerene MAb with carbon nanotubes, detection was poor. We are now working on the optimization of the method at this point.

Relationship to the work of others: One of our detection methods takes advantage of the inherent Raman peak of the graphite structure in CNTs to quantitate them in different excised tissue samples without adding radioactive isotopes that could potentially influence their biodistribution. In addition, the modification of CNTs with DOTA (1,4,7,10-tetraazacyclododecane-1,4,7,10- tetraacetic acid) metal chelator is difficult to prepare; and the radiolabeling procedure can be costly and time-consuming involving unnecessary exposure to radiation. Our Raman imaging method is consistent with previous reports (5).

We have attempted to develop additional methods of quantifying the amount of CNTs present in tissues. We are in the final stages of optimizing our methods using dynabeads and anti-fullerene monoclonal antibody.

KEY RESEARCH ACCOMPLISHMENTS:

CNTs attached to MAbs for targeting and photothermal ablation of tumor cells are:

- Well-dispersed and retained their optical properties;
- The MAb-CNT conjugates are chemically stable
- The conjugates bound specifically to target cells and binding remained specific even after the MAb-CNTs were incubated in mouse serum;
- Specifically targeted cells can be thermally ablated following exposure to NIR light.

REPORTABLE OUTCOMES:

Papers:

1. Chakravarty P, Marches R, Zimmerman NS, Swafford AD, Bajaj P, Musselman IH, Pantano P, Draper RK, Vitetta ES. Thermal ablation of tumor cells with antibody-functionalized single-walled carbon nanotubes. *Proc. Natl. Acad. Sci. USA.* 105: 8697-702, 2008.

2. Marches R, Chakravarty P, Musselman IH, Azad, R, Draper RK, Vitetta ES. Selective thermal ablation of tumor cells using a monoclonal antibody covalently coupled to single-wall carbon nanotubes. *Int. J. Cancer (in press) DOI: 10.1002/ijc.24659*.

3. Wang R, Mikoryak C, Chen E, Li S, Pantano P, Draper RK. A sensitive gel electrophoresis method to measure the concentration of single-walled carbon nanotubes *(submitted)*

Presentations:

1. Swafford AD, Chakravarty P, Dieckmann G, Draper RK, Musselman IH, Pantano P, Marches R, Vitetta ES. Isolation and analysis of MAb/Single-walled carbon nanotube complexes by ultracentrifugation in iodixanol. STARS presentation forum, UT Southwestern Medical Center, 2007.

Grants:

1. Texas Advanced Research (Biological Sciences) Program grant No. 009741-0005-2007 – Antibody-conjugated carbon nanotubes for selective photothermal ablation of human tumors (2007).

2. NIH R01 - Her2 targeted carbon nanotubes for photothermal ablation of breast tumors- *Application Number:* NIH R01 CA138813-01 (2008).

Ph.D. students:

1. Pavitra Chakravarty – Bioengineering, - UT Arlington. / UT Southwestern Medical Center

CONCLUSION:

The in vitro studies indicate a good selectivity of thermal ablation achieved with MAb-targeted CNTs following exposure to NIR light. The MAb-CNTs do not have any obvious inherent cytotoxicity and are relatively stable in mouse serum. The covalent MAb-CNTs might present an advantage over the noncovalent ones for *in vivo* treatments in terms of stability/specificity. However, final conclusions will be reached after the biodistribution, pharmacokinetics and animal toxicity tests are completed.

REFERENCES:

1. Kam NW, O'Connell M, Wisdom JA, Dai H. Carbon nanotubes as multifunctional biological transporters and near-infrared agents for selective cancer cell destruction. *Proc Nat Acad Sci* 102: 11600-11605, 2005.
2. Shao N, Lu S, Wickstrom E, Panchapakesan B. Integrated molecular targeting of IGF1R and Her2 surface receptors and destruction of breast cancer cells using single wall carbon nanotubes. *Nanotechnol* 18: 315101-315109, 2007.
3. Welsher K, Liu Z, Daranciang D, Dai H. Selective probing and imaging of cells with single walled carbon nanotubes as near-infrared fluorescent molecules. *Nano Lett* 8: 586-590, 2008.
4. Cherukuri P, Gannon CJ, Leeuw TK, Schmidt HK, Smalley RE, Curley SA, Weisman RB. Mammalian pharmacokinetics of carbon nanotubes using intrinsic near-infrared fluorescence. *Proc Natl Acad Sci USA.* 103: 18882-18886, 2006.
5. Liu Z, Cai W, He L, Nakayama N, Chen K, Sun X, Chen X, Dai H. *In vivo* biodistribution and highly efficient tumor targeting of carbon nanotubes in mice. *Nat Nanotechnol.* 2: 47-52, 2007.
6. Schipper ML, Nakayama-Ratchford N, Davis CR, Kam NW, Chu P, Liu Z, Sun X, Dai H, Gambhir SS. A pilot toxicology study of single-walled carbon nanotubes in a small sample of mice. *Nat Nanotechnol.* 3: 216-221, 2008.
7. Sayes CM, Fortner JD, Guo W, Lyon D, Boyd AM, Ausman KD, Tao YJ, Sitharaman B, Wilson LJ, Hughes JB, West JL, Colvin VL. The differential cytotoxicity of water soluble fullerenes. *Nano Lett.* 4: 1881-1887, 2004.
8. Coleman KS, Azamian BR, Davis JJ, Bagshaw CB, Green MLH. Chemistry, biochemistry, and electrochemistry of single-walled carbon nanotubes. *Pap Am Chem S* 224: U420-U421, 2002.
9. Bianco A, Kostarelos K, Partidos CD, Prato M. Biomedical applications of functionalized carbon nanotubes. *Chem Commun.* 571-577, 2005.
10. Lin Y, Taylor S, Li HP, Fernando KAS, Qu LW, Wang W, Gu LR, Zhou B, Sun YP. Advances toward bioapplications of carbon nanotubes. *J Mater Chem.* 14: 527-541, 2004.
11. Huang W, Taylor S, Fu K, Lin Y, Zhang D, Hanks TW, Rao AM, Sun Y. Attaching proteins to carbon nanotubes *via* diimide-activated amidation. *Nano Lett.* 2: 311-314, 2002.
12. Zhao W, Song C, Pehrsson PE. Water-soluble and optically pH-sensitive single-walled carbon nanotubes from surface modification. *J Am Chem Soc.* 124: 12418-12419, 2002.
13. McDevitt MR, Chattopadhyay D, Kappel BJ, Jaggi JS, Schiffman SR, Antczak C, Njardarson JT, Brentjens R, Scheinberg DA. Tumor targeting with antibody-functionalized, radiolabeled carbon nanotubes. *J Nucl Med.* 48: 1180-1189, 2007.
14. Wang Y, Iqbal Z, Mitra S. Rapidly functionalized, water-dispersed carbon nanotubes at high concentration. *J Am Chem Soc.* 128: 95-99, 2006.
15. Liu Z, Sun X, Nakayama-Ratchford N, Dai H. Supramolecular chemistry on water-soluble carbon nanotubes for drug loading and delivery. *ACS Nano* 1: 50-56, 2007.
16. Weissleder R. A clearer vision for *in vivo* imaging. *Nat Biotechnol.* 19: 316-317, 2001.
17. Gobin AM, Lee MH, Halas NJ, James WD, Drezek RA, West JL. Near-infrared resonant nanoshells for combined optical imaging and photothermal cancer therapy. *Nano Lett.* 7: 1929-1934, 2007.
18. Loo C, Lowery A, Halas N, West J, Drezek R Immunotargeted nanoshells for integrated cancer imaging and therapy. *Nano Lett* 5: 709-711, 2005.
19. Huang X, El-Sayed IH, Qian W, El-Sayed MA. Cancer cell imaging and photothermal therapy in the near-infrared region by using gold nanorods. *J Am Chem Soc* 128: 2115-2120, 2006.

20. Hirsch LR, Stafford RJ, Bankson JA, Sershen SR, Rivera B, Price RE, Hazle JD, Halas NJ, West JL. Nanoshell-mediated near-infrared thermal therapy of tumors under magnetic resonance guidance. *Proc Natl Acad Sci USA.* 100: 13549-13554, 2003.

21. Ghetie MA, Picker LJ, Richardson JA, Tucker K, Uhr JW, Vitetta ES. Anti-CD19 inhibits the growth of human B-cell tumor lines in vitro and of Daudi cells in SCID mice by inducing cell cycle arrest. *Blood.* 83: 1329-1336, 1994.

22. Marches R, Scheuermann RH, Uhr JW. Cancer dormancy: role of cyclin-dependent kinase inhibitors in induction of cell cycle arrest mediated via membrane IgM. *Cancer Res.* 58: 691-697, 1998.

23. Braden BC, Goldbaum FA, Chen B, Kirschner AN, Wilson SR, Erlanger BF. X-ray crystal structure of an anti-buckminsterfullerene antibody Fab fragment: biomolecular recognition of C_{60}. *Proc Nat. Acad Sci USA.* 97: 12193-12197, 2000.

24. Erlanger BF, Chen B, Zhu M, Brus L. Binding of an anti-fullerene IgG monoclonal antibody to single wall carbon nanotubes. *Nano Lett.* 1: 465-467, 2001.

APPENDICES:

Personnel paid from grant:

VITETTA, ELLEN SHAPIRO

BARRON, PHYLLIS

CHAKRAVARTY, PAVITRA

MAPES, KELLY ANN

MARCHES, RADU GERVIN

WILLINGHAM, DAVID RYAN

WOZNIAKOWSKI, ANETA

Articles from grant:

Thermal ablation of tumor cells with antibody-functionalized single-walled carbon nanotubes - *www.pnas.org_cgi_doi_10.1073_pnas.0803557105*

Specific thermal ablation of tumor cells using single-walled carbon nanotubes targeted by covalently-coupled monoclonal antibodies - *Int. J. Cancer*

Thermal ablation of tumor cells with antibody-functionalized single-walled carbon nanotubes

Pavitra Chakravarty*†, Radu Marches*†, Neil S. Zimmerman‡, Austin D.-E. Swafford§, Pooja Bajaj¶, Inga H. Musselman¶‖, Paul Pantano¶‖, Rockford K. Draper§¶‖, and Ellen S. Vitetta*,**

*The Cancer Immunobiology Center, University of Texas Southwestern Medical Center, Dallas, TX 75390; ‡Department of Biological Engineering, Massachusetts Institute of Technology, Cambridge, MA 02139; and ‖The Alan G. MacDiarmid NanoTech Institute and Departments of §Molecular and Cell Biology and ¶Chemistry, University of Texas at Dallas, Richardson, TX 75080

Contributed by Ellen S. Vitetta, April 11, 2008 (sent for review April 1, 2008)

Single-walled carbon nanotubes (CNTs) emit heat when they absorb energy from near-infrared (NIR) light. Tissue is relatively transparent to NIR, which suggests that targeting CNTs to tumor cells, followed by noninvasive exposure to NIR light, will ablate tumors within the range of NIR. In this study, we demonstrate the specific binding of antibody-coupled CNTs to tumor cells *in vitro*, followed by their highly specific ablation with NIR light. Biotinylated polar lipids were used to prepare stable, biocompatible, noncytotoxic CNT dispersions that were then attached to one of two different neutralite avidin-derivatized mAbs directed against either human CD22 or CD25. $CD22^+CD25^-$ Daudi cells bound only CNTs coupled to the anti-CD22 mAb; $CD22^-CD25^+$ activated peripheral blood mononuclear cells bound only to the CNTs coupled to the anti-CD25 mAb. Most importantly, only the specifically targeted cells were killed after exposure to NIR light.

immunoconjugates | lymphoma cells | monoclonal antibodies | nanotechnology | near infrared light

Despite the success of current treatments for several types of cancer, all known treatments have major limitations. Conventional chemotherapy or radiotherapy damage many cells, and both have significant side effects. In addition, tumor cells develop resistance to many chemotherapeutic agents (1), and most chemotherapeutic drugs kill dividing cancer cells and not dormant ones. To decrease nonspecific toxic effects and kill nondividing cells, targeted therapies are being developed and some have already been approved by the Food and Drug Administration for use in humans. These include both small molecules that target specific intracellular pathways in tumor cells and mAbs that target molecules on their surface. Some of these targeted agents are cytostatic and not cytotoxic, and they are often given in combination with chemotherapy in an effort to both lower the dose of chemotherapy required and hence reduce side effects and achieve additive or synergistic effects. With regard to mAbs, strategies include increasing cytotoxicity by coupling them to drugs, radionuclides, toxins, drugs, or prodrugs (2, 3). These agents (collectively called immunoconjugates) are potent, and three have been approved for human use (4, 5). However, they also have side effects because they carry toxic payloads. We and others have successfully tested the antitumor activity of different agents, including signaling antibodies and immunotoxins, alone or in combination with pharmacological agents, in disseminated or solid human tumors grown in immunocompromised mice (5–9). We have also tested four different immunotoxins in humans (10–15). To optimize the use of mAbs in cancer therapy, it is important to explore their use with new types of payloads and carriers, including carbon nanotubes (CNTs). The ability of CNTs to convert near-infrared (NIR) light into heat provides an opportunity to create a new generation of immunoconjugates for cancer photo-therapy with high performance and efficacy. Moreover, hyperthermia has been clinically used in the management of solid tumors because it can synergistically enhance tumor cytotoxicity when combined with chemotherapy or radiotherapy (16, 17). Hyperthermia also preferentially increases the permeability of tumor vasculature compared with normal vasculature, which can enhance the delivery of drugs into tumors. Therefore, the thermal effects generated by targeted CNTs may have important advantages. Recent pharmacokinetic studies have reported that CNTs dispersed by different procedures lack nonspecific toxic effects in mice (18–20).

The use of NIR-resonant nanostructures, including gold nanoshells and CNTs, to thermally ablate cancer cells is being explored by several groups (21–26). The use of NIR light in the 700- to 1,100-nm range for the induction of hyperthermia is particularly attractive because living tissues do not strongly absorb in this range (27). Hence, an external NIR light source should effectively and safely penetrate normal tissue and ablate any cells to which the CNTs are attached. The critical aspect for selective CNT-mediated thermal ablation of cells is to stably attach targeting moieties that will not interfere with the optical properties of the CNTs and yet retain targeting specificity. The targeting of CNTs to tumor cells can be accomplished by coating them with cell-binding ligands such as peptides or mAbs (25, 26, 28–30). Several studies have reported that the targeting of such CNTs is "specific" (25, 26, 29, 30), but no study has used both a control ligand and a control cell to convincingly demonstrate ligand-specific thermal ablation of tumors cells with CNTs. Specificity is critical because nonspecific binding to antigen-negative cells *in vivo* could cause major side effects, which has been a confounding issue in the cancer targeting field for >25 years.

The aim of this study was to design and prepare an anti-CD22-targeted CNT construct to ablate human Burkitt's lymphoma cells *in vitro*. Herein, we describe the physical properties of these CNT constructs, their selective binding to tumor cells, and the NIR-induced thermal ablation of the targeted tumor cells. Importantly, both a control CNT construct and a control cell were used to definitely prove specificity.

Results

Dispersion of CNTs. Well dispersed single-walled CNTs were prepared by sonicating CNTs in the presence of 1,2-distearoyl-

Author contributions: P.C., R.M., and E.S.V. designed research; P.C. and R.M. performed research; P.C., R.M., I.H.M., P.P., R.K.D., and E.S.V. analyzed data; and P.C., R.M., N.S.Z., A.D.-E.S., I.H.M., P.P., R.K.D., and E.S.V. wrote the paper.

Conflict of interest statement: E.S.V., R.K.D., P.P., and I.H.M. are affiliated with Medical Nanotechnologies, Inc. E.S.V. is a coinventor on an issued patent encompassing this work.

†P.C. and R.M. contributed equally to this work.

**To whom correspondence should be addressed. E-mail: ellen.vitetta@utsouthwestern.edu.

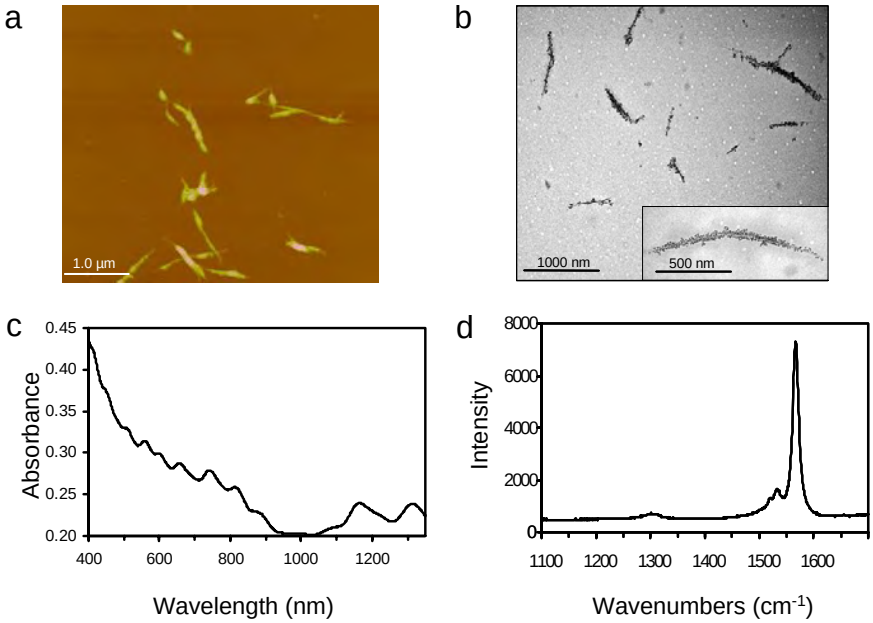

Fig. 1. Water-soluble CNTs functionalized with biotinylated polar lipids. (*a*) AFM image of B-CNTs shows CNTs coated by the biotinylated polar lipid, DSPE-PEG-biotin. (*b*) TEM images of individual B-CNTs show uniform coverage of biotin after immunodetection with gold-labeled anti-biotin. (*Inset*) Higher magnification of a B-CNT coated with gold-labeled antibiotin. (*c*) UV-Vis-NIR spectrum of B-CNTs show a number of metallic and semiconducting CNT absorbances consistent with the presence of individual tubes. (*d*) Raman spectra of B-CNTs show an intense G band (≈1,590 cm^{-1}) indicating the presence of CNTs. In all cases, one representative experiment of at least three independent experiments is shown.

sn-glycero-3-phosphoethanolamine-*N*-[biotinyl(polyethylene glycol) 2000] [DSPE-PEG(2000)-biotin], followed by centrifugation to recover the biotinylated CNTs (B-CNTs). The resulting B-CNT suspension contained 0.06 mg CNT/ml and ≤3 parts per million metals, as determined by thermal gravimetric analysis (TGA) and inductively coupled plasma mass spectrometry (MS) (data not shown). The dispersions were stable and did not aggregate at room temperature for >120 days. Atomic force microscopy (AFM) analysis demonstrated that the suspension was free of nontubular carbon structures and the CNTs were either individually dispersed or in small bundles. The lengths of the CNTs ranged from 0.2 to 1.4 μm with an average of 0.59 μm (Fig. 1*a*). Analysis by transmission electron microscopy (TEM) of the B-CNT samples probed with gold-labeled goat antibiotin demonstrated that biotin was distributed along the entire surface of the B-CNT (Fig. 1*b*). The biotin content of the B-CNT dispersion was determined by using a competitive ELISA and adding dilutions of the B-CNT dispersion to biotin-HRP and plating them onto neutralite avidin (NA)-coated plates. The amount of HRP-labeled biotin was detected by the development of color in the presence of the 2,2′-azino-bis(3-ethylbenzothiazoline-6-sulfonic acid) (ABTS) substrate. Using this assay, we found that the content of biotin was 0.02 mmol/g of B-CNT. The UV-visible (Vis)-NIR spectra of the B-CNTs confirmed the quality of these dispersions with the presence of electronic transitions between van Hove singularities, suggesting that the optical properties of the CNTs were maintained after the adsorption of DSPE-PEG-biotin (Fig. 1*c*). The Raman spectra of the B-CNTs showed a number of well characterized CNT resonances such as the radial breathing mode region between 100 and 300 cm^{-1} (data not shown) and the tangential (G-band) peak at 1,590 cm^{-1}, confirming the presence of CNTs in the sample (Fig. 1*d*).

To determine whether B-CNTs were inherently cytotoxic (in the absence of NIR), cells from the IgM^+ $CD22^+CD25^-$ Burkitt's lymphoma cell line Daudi were incubated for 24 h with up to the highest amount of B-CNTs used in the binding and killing assays (3.6 μg). No toxicity was observed using a [^{3}H]thymidine incorporation assay (data not shown).

Preparation of mAb-NA Targeting Moieties. To prepare the targeting agents, we coupled NA to mAbs. To this end, mouse IgG anti-human CD22 (RFB4) or mouse IgG anti-human CD25 (RFT5) were thiolated with 2-iminothiolane (Traut's reagent). NA was activated with *m*-maleimidobenzoyl-*N*-hydroxysuccinimide ester (MBS). Then, the purified thiolated IgG was mixed with MBS-activated NA at a 2:1 ratio as shown by preliminary experiments to give the best yields as determined by the elution profile of the resulting conjugate on a Sephacryl S-300 HR column (Fig. 2*a*). The concentration of the mAb-NA conjugates was determined by using the bicinchoninic acid assay (BCA). Both mAb-NA conjugates were free of impurities as judged by Western blot analysis (Fig. 2*a*). We next determined whether these conjugates were cytotoxic to Daudi cells after incubation of cells for 24 h with up to 10 μg/ml of RFB4-NA; cytotoxicity was determined by [^{3}H]thymidine incorporation. Similar concentrations of unconjugated RFB4 and NA were used as negative controls, and goat anti-IgM (which induces apoptosis of Daudi cells) (31) was used as the positive control. We found that the RFB4-NA conjugates were not cytotoxic, whereas (as predicted) the goat anti-IgM reduced [^{3}H]thymidine incorporation by >50% (Fig. 2*b*).

The specific binding of RFB4-NA and RFT5-NA conjugates to $CD22^+CD25^-$ Daudi cells and $CD22^-CD25^+$ phytohaemagglutinin (PHA)-activated peripheral blood mononuclear cells (PBMCs), respectively, was demonstrated by flow cytometry, using either FITC-labeled goat anti-mouse Ig (GAMIg) or FITC-biotin (data not shown for FITC-biotin). The latter was confirmed by the ability of the cell-bound mAb-NA to bind to B-CNT. Daudi cells were precoated with a saturating concentration of RFB4-NA, washed, and incubated with increasing amounts of B-CNTs. The RFB4-NA, but not the RFT5-NA conjugate could target an average of 0.237 pg of B-CNTs per cell (Fig. 2*c*).

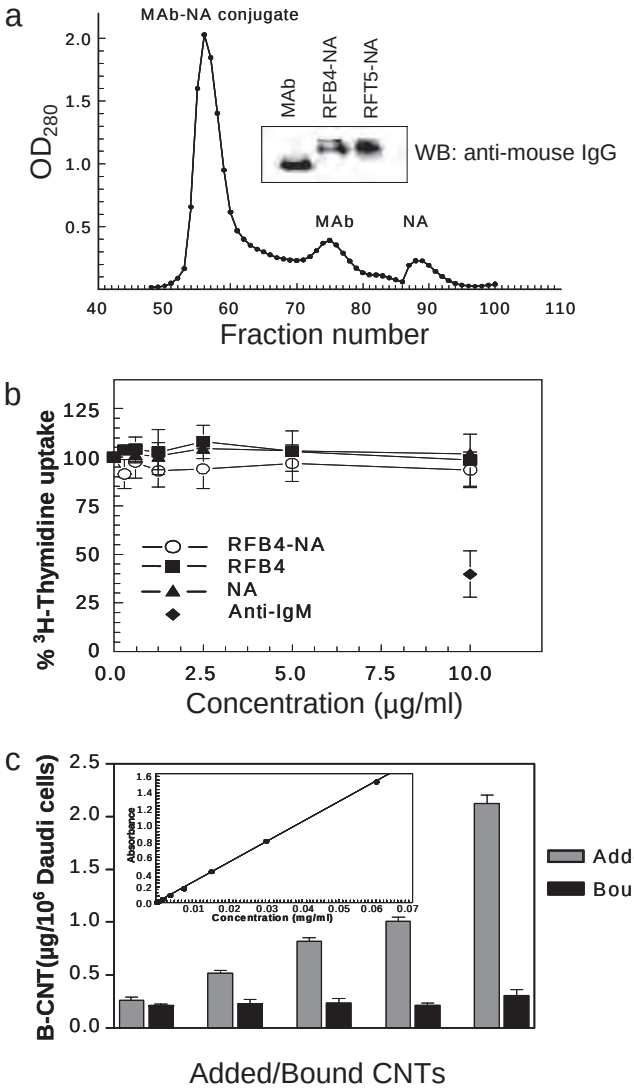

Fig. 2. Analysis of mAb-NA conjugates. (*a*) A typical chromatographic separation of RFB4-NA from unconjugated RFB4 and NA using a Sephacryl S-300 HR column. Fractions of the first peak containing the RFB4-NA conjugate were pooled and concentrated. (*Inset*) Purified RFB4-NA, RFT5-NA, or mAb were electrophoresed under nondenaturing conditions on a 7.5% polyacrylamide gel and immunoblotted with HRP-labeled sheep anti-mouse IgG. Data in *a* are representative of at least three independent experiments. (*b*) A total of 5×10^4 Daudi cells were incubated for 24 h with increasing amounts of the RFB4-NA conjugate, and cytotoxicity was detected by [^{3}H]thymidine incorporation. Similar concentrations of unconjugated RFB4 or NA were used as negative controls, whereas 10 μg/ml goat anti-IgM was used as positive control. Data represent mean ± SD of three independent experiments. (*c*) One million Daudi cells precoated with a saturating concentration of RFB4-NA were incubated with increasing amounts of B-CNT. Saturating concentration of RFB4-NA can target 0.237 pg of B-CNT per Daudi cell. No detectable B-CNT binding was found on uncoated cells or cells precoated with RFT5-NA (control). Data represent mean ± SD of three independent experiments.

Preparation and Testing of mAb-CNT Complexes. We next prepared the mAb-CNT conjugates by coupling the B-CNTs to either RFB4-NA or RFT5-NA for 35 min at room temperature. After the removal of the supernatant containing the unreacted mAb-NA, the optical properties of the freshly prepared mAb-CNT were tested. The UV-Vis-NIR spectra of the mAb-CNT conjugates displayed the same metallic and semiconducting CNT types as observed for the B-CNTs, indicating that the optical properties of the CNTs were not affected by the coupling (Fig. 3*a*), and the characteristic CNT resonances displayed in the Raman spectra of the mAb-CNTs again confirmed the presence of CNTs in the sample (Fig. 3*b*).

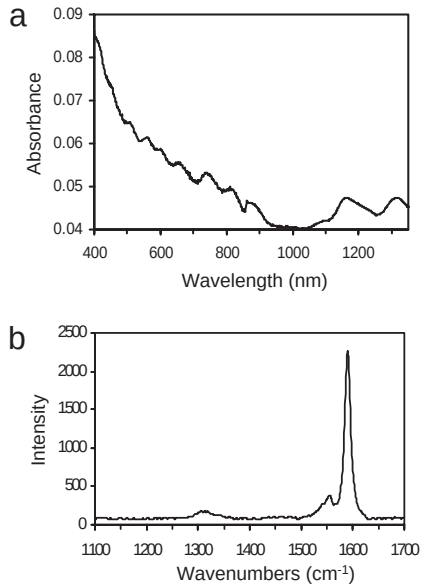

Fig. 3. Optical properties of CNTs following coupling with mAbs (mAb-CNT). (*a*) UV-Vis-NIR spectrum of RFB4-CNTs show the same metallic and semiconducting CNT types as observed for the B-CNTs, indicating the retention of the optical properties of CNTs after the coupling with RFB4-NA. The sharp feature at 861 nm is caused by a grating and detector change associated with the spectrometer. (*b*) Raman spectrum of RFB4-CNTs show an intense G band (≈1,590 cm^{-1}) as the B-CNTs, indicating the presence of CNTs in the conjugate. The spectra are representative of three independent experiments.

The ability of the mAb-CNT conjugates to bind to antigen-positive but not antigen-negative target cells was assessed by flow cytometry. The components of the cell-bound mAb-CNT were detected by using FITC-GAMIg (which binds to mouse mAb) and phycoerythrin-streptavidin (PE-SA) (which binds to biotin), respectively. We found that RFB4-CNT and RFB4 (positive control) bound equally well to Daudi cells, whereas RFT5-CNT (negative control) bound poorly ($P < 0.001$) (Fig. 4*a*). Conversely, RFT5-CNT and RFT5 bound equally well to $CD22^-CD25^+$ PHA-activated PBMCs (95% $CD25^+$ cells), whereas the negative control conjugate, RFB4-CNT, did not ($P < 0.002$) (Fig. 4*b*). These results demonstrate that the coupling of the mAbs to CNTs does not alter their mAb-binding activity and that the mAb-CNTs bind to antigen-expressing cells as specifically as the uncoupled mAbs.

Having demonstrated that the mAb-CNT conjugates retained the binding activity of the mAb and the optical properties of the CNTs, we next determined whether cells targeted by the mAb-CNTs could be thermally ablated after exposure to NIR light. Cells were incubated with the mAb-CNTs in PBS, washed three times with PBS, and then dispensed into 96-well plates in cell culture media. The cells in the plate were exposed to an 808-nm laser (5 W/cm^2) for 7 min and pulsed for the next 12 h with 1 μCi [^{3}H]thymidine to assess cell viability. As shown in Fig. 5*a*, as compared with treatment with the nonbinding RFT5-CNTs, the viability of the RFB4-CNT-treated Daudi cells was significantly reduced after exposure to NIR light ($P < 0.0001$). Conversely, when activated PBMCs were used as target cells, RFT5-CNT, but not RFB4-CNT, killed the cells after exposure to NIR light ($P < 0.0001$) (Fig. 5*b*). These experiments demonstrate that the binding of the mAb-CNTs to their respective antigen-positive target cells leads to their specific ablation after exposure to NIR light.

MEDICAL SCIENCES

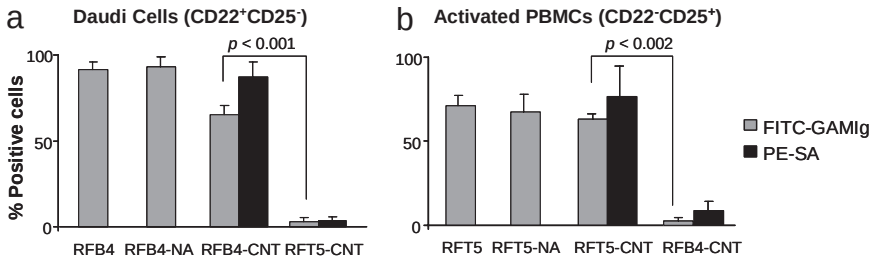

Fig. 4. Binding of mAb-CNTs to target cells. One million cells were incubated with saturating concentrations of RFB4-CNTs or RFT5-CNTs and then incubated either with FITC-GAMIg to detect the mAbs or with PE-SA to detect the B-CNTs and analyzed on a FACScan. (*a*) The specific binding of RFB4-CNTs to Daudi cells using RFT5-CNTs as a negative control ($P < 0.001$). (*b*) The specific binding of RFT5-CNT to activated PBMCs (>95% T cells) using RFB4-CNT as a negative control ($P < 0.002$). Data represent mean ± SD of at least three independent experiments.

Because we anticipate using these mAb-CNTs *in vivo*, it was important to demonstrate that they retained activity in serum at 37°C. Therefore, the mAb-CNTs were incubated in mouse serum at 37°C for 0, 24, 48, and 72 h. At each time point, the mAb-CNTs were washed with PBS, incubated with Daudi cells, and irradiated with NIR light in a procedure similar to the thermal ablation described above. No loss in their ability to thermally ablate Daudi cells was observed, even after 72 h in mouse serum at 37°C (Fig. 5*c*).

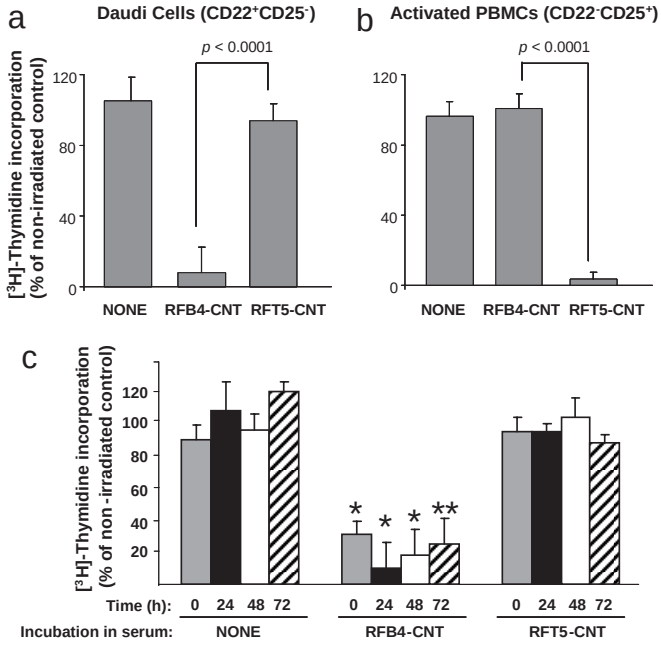

Fig. 5. Ablation of mAb-CNT-coated cells with NIR. One million cells were incubated with saturating concentrations of RFB4-CNTs or RFT5-CNTs. Cells were dispensed into 96-well plates, exposed for 7 min to 808-nm NIR light (5 W/cm^2), pulsed with 1 μCi [^{3}H]thymidine, and harvested 12 h later. The incorporated radioactivity was measured by liquid scintillation counting from triplicate samples. The percentage of radioactivity incorporated by each sample was calculated relative to corresponding nonirradiated sample. (*a*) The specific killing by RFB4-CNTs of Daudi cells using RFT5-CNTs as a negative control ($P < 0.0001$). (*b*) The specific killing of RFT5-CNT on activated PBMCs (>95% T cells) using RFB4-CNTs as a negative control ($P < 0.0001$). Data represent mean ± SD of at least three independent experiments. (*c*) The stability of the mAb-CNTs *in vitro* was determined by incubating them in mouse serum at 37°C for 0, 24, 48, and 72 h. At each time point, the mAb-CNTs were washed with PBS, incubated with Daudi cells, and exposed to NIR light as described above. The activity of the RFB4-CNTs at the different time points remained unchanged. *, $P < 0.0001$; **, $P < 0.05$ for the values obtained at the corresponding time points with RFT5-CNTs. Data represent mean ± SD of three independent experiments.

Discussion

The first critical challenge in the field of targeted CNTs is to create soluble and stable CNTs that retain both the specificity of the targeting moiety and the thermal activity of the CNTs even in serum at physiological temperatures. In this article, we demonstrate that this can be accomplished. Our strategy involved the generation of targeting moieties consisting of mAb-NAs attached to dispersed biotinylated CNTs. The use of B-CNTs and mAb-NAs gives us the flexibility to "assemble" the targeted CNTs by using any cell-binding mAb. Second, the one-step strategy of generating dispersed CNTs by using biotinylated polar lipids has the advantage of preventing subsequent chemical treatments that remove the polar lipids and/or destroy their optical properties. Of equal importance is the specificity of the targeting strategy. Thus, previous studies have demonstrated that folic acid-coated CNTs could be targeted to folate receptor (FR)-positive cells and that NIR light killed the cells (25). Although FR-negative cells were used as a control, CNTs coated with an irrelevant ligand were not. In other studies, rArg-Gly-Asp (RGD)-CNTs were used to deliver adsorbed doxorubicin (29). These CNTs were also evaluated for *in vivo* biodistribution (19), but control peptide-CNTs were not used to demonstrate specificity. Another approach for targeting CNTs to cells is to noncovalently attach mAbs that can be used in photothermal therapy (26) or imaging (30). However, attachment of mAbs by direct adsorption on CNTs involves a potential loss of the targeting function of the mAbs and, indeed in the study cited, specificity controls were not reported, and cell viability studies showed 50% collateral damage by the irrelevant mAb-CNT control after exposure to NIR light (26). In another very elegant study, mAbs were covalently attached to CNTs to deliver radionuclides to cells (28). These studies achieved their goal of killing target cells by radiotherapy and showed both linkage stability and specific targeting. However, because the objective of these studies was not to ablate cells with NIR light, we do not know whether the optical properties of the CNTs were preserved.

Having demonstrated excellent specificity of both targeting and thermal ablation *in vitro*, the next step is to evaluate the pharmacokinetics, biodistribution, toxicity, and activity of these mAb-CNT constructs *in vivo*.

Materials and Methods

Materials. Purified CNTs (HiPco) were purchased from Carbon Nanotechnologies. The polar lipid DSPE-PEG(2000) biotin was purchased from Avanti Polar Lipids. Mouse IgG1 anti-human CD22 (RFB4) and mouse IgG anti-human CD25 (RFT5) were prepared and purified in our laboratory at UT Southwestern Medical Center. Traut's reagent and MBS were purchased from Pierce/Endogen. NA was purchased from Accurate Chemical and Scientific.

Cell Culture. Daudi cells (American Type Culture Collection) were cultured in RPMI 1640 medium (Sigma) containing 1% antibiotic-antimycotic mixture (penicillin/streptomycin/Amphotericin B) (Sigma), 10% heat-inactivated FCS (HyClone), and 2 mM L-glutamine (Sigma) (complete medium). PBMCs from

normal healthy donors were isolated from the fresh heparinized blood by Ficoll-Paque PLUS (GE Healthcare) density gradient centrifugation. Normal activated $CD25^+$ cells were generated by culturing the PBMCs for 72 h at 1×10^6 cells/ml in complete medium supplemented with 5 μg/ml PHA (Sigma).

CNT Solubilization by Biotinylated Polar Lipids and Characterization. Degassed ultrapure deionized (DI) water was used for all solutions. CNTs (0.3 mg) were suspended in 1 ml of 166 μM DSPE-PEG(2000)-biotin. The mixture was sonicated with a 2-mm probe tip connected to a Branson Sonifier 250 (VWR) for 10 min at a power level of 10 W, with the sample immersed in an ice water bath. To remove excess DSPE-PEG-biotin, samples were washed twice in DI water by centrifugation for 15 min at 90,000 $\times$ *g* at 4°C. The supernatant was discarded, the pellet was resuspended in 1 ml of DI water, and the procedure was repeated. The samples were then centrifuged two times for 10 min at 16,000 $\times$ *g* at room temperature, and the upper 50% of the supernatant containing the B-CNT was recovered. To obtain more concentrated samples, the B-CNT suspension was centrifuged for 60 min at 16,000 $\times$ *g* at 4°C, the supernatant was discarded, and the pellet was resuspended in 0.2 ml of DI water.

Sample concentration was detected by TGA using a Pyris-1 thermal gravimetric analyzer (PerkinElmer) equipped with a high-temperature furnace and sample thermocouple. AFM was performed in air under ambient conditions by using a Digital Instruments Nanoscope III Multimode scanning probe microscope (Veeco Metrology). Images were acquired in the TappingMode by using cantilevers with 0.9 Nm^{-1} force constants as described (32). A dual-beam Lambda 900 UV-Vis-NIR spectrophotometer (PerkinElmer) with a scan speed of 25 nm/min and a 0.4-s integration time was used for absorption spectra. Raman spectroscopy at 633-nm excitation was performed with a LabRAM high-resolution confocal Raman microscope system (Jobin Yvon). Wave number calibration was performed by using the 520.5-cm^{-1} line of a silicon wafer; the spectral resolution was $\approx$1 cm^{-1} as described (33). TEM was performed with a JEOL JEM-1200EX II electron microscope. The B-CNT dispersion was probed with 5-nm gold beads labeled with goat antibiotin (Kirkegaard & Perry Laboratories), and then imaged.

Preparation of mAb-NA Conjugates. To couple the B-CNTs to mAbs, we used a modified protocol (34). Briefly, 10 mg of RFB4 or RFT5 in 1 ml of 0.15 M borate buffer, 0.1 mM EDTA, pH 8.5 were thiolated by incubation for 1 h at room temperature with a 20:1 molar excess of Traut's reagent. After incubation, the reaction was quenched with 0.1 M glycine. In parallel, 10 mg of NA dissolved in 1 ml of 0.01 M PBS, 0.1 mM EDTA, pH 7.4, was activated by 30-min incubation at room temperature by using a 6:1 molar excess of MBS. The unreacted Traut's reagent and MBS were removed by gel filtration on Sephadex G-25 columns in 0.01 M PBS, 0.1 mM EDTA, pH 7.4. The thiolated mAb was conjugated to the activated NA at a molar ratio of 1:2 for 2 h at room temperature with gentle shaking. The resultant conjugate was purified by gel filtration on a Sephacryl S-300 HR column (GE Healthcare) by using 0.1 M PBS, 0.05% Tween-20, pH 7.4. The protein concentration in the purified conjugate was quantified by using the BCA assay (Pierce/Endogen). The size and integrity of the conjugate was analyzed by Western blot. The samples were electrophoresed on a 7.5% nondenaturing polyacrylamide gel and transferred to PVDF membranes (Bio-Rad), probed with HRP-labeled sheep anti-mouse IgG, and visualized by using an enhanced chemiluminescence system (GE Healthcare).

Competition ELISA. NA-coated 96-well plates were blocked with 1% BSA in 0.01 M PBS, 0.05% Tween-20 (PBST) for 1 h. B-CNTs were added to each well together with biotin-labeled HRP and incubated for 1 h. After washing five times with PBST, the substrate ABTS was added, and absorbance was measured at 405 nm. The amount of biotin bound to the CNTs (biotin mmol/μg B-CNT) was calculated by using a standard curve constructed by plotting OD against the biotin concentration (ng/ml) prepared by coincubating increasing amounts of biotin in the presence of a constant amount of HRP-biotin. A similar procedure was used to detect the amount of NA in mAb-NA conjugates.

Preparation of mAb-CNT Conjugate. Fresh mAb-CNTs were prepared immediately before use by mixing B-CNT with mAb-NA in a 1:2 (wt/wt) ratio. The mixture was placed on a rocker for 35 min at room temperature and vortexed gently every 5 min. After coupling, the mixture was centrifuged for 5 min at 16,000 $\times$ *g* at 4°C, the supernatant containing unreacted mAb-NA was discarded, and the pellet was resuspended in 40 μl of PBS for every 3.6 μg of B-CNT and used immediately.

Binding of mAb-CNTs to Target Cells. One million Daudi cells or PHA-activated PBMCs (>95% $CD25^+$ cells) were incubated with the mAb-CNTs for 20 min at 4°C in PBS. Cells were washed two times with ice-cold PBS and then incubated with either PE-SA (Jackson ImmunoResearch) or FITC-GAMIg (Kirkegaard & Perry Laboratories) for 20 min at 4°C. The cells were washed two times with ice-cold PBS and resuspended in 0.5 ml of PBS, and the bound fluorescence was analyzed on a FACScan (Becton Dickinson).

Determination of the Amount of B-CNTs Bound per Cell. One million Daudi cells were incubated with saturating amounts of RFB4-NA or RFT5-NA for 15 min at 4°C in PBS. Cells were washed two times with ice-cold PBS, incubated with incremental amounts of B-CNT for 20 min at 4°C in PBS, and then washed two times with ice-cold PBS. The amount of B-CNT bound to cells was determined by measuring the absorbance at 808 nm of the B-CNT suspension before and after incubation with Daudi cells. The amount of B-CNT bound per cell was determined by using the extinction coefficient [$\varepsilon^{0.1\%} = 25$ $(mg/ml)^{-1}$] calculated from the linear fit (Beer-Lambert law) of absorbance at 808 nm versus the B-CNT concentration.

Ablation of mAb-CNT-Coated Cells with NIR Light. One million cells were incubated with 40 μl of the mAb-CNTs in PBS for 20 min at 4°C. Cells were washed three times with ice-cold PBS, and then 10^5 cells were dispensed in triplicate wells in a 96-well plate in 200 μl of complete medium. The cells were exposed to continuous NIR light by using a FAP-Sys-30W 805- to 811-nm laser system (Coherent) for 7 min at 5 W/cm^2. Cell death was assessed by pulsing the cells for the next 12 h with 1 μCi [^{3}H]thymidine per well, and the incorporated radioactivity was measured by liquid scintillation counting. The incorporated radioactivity for each sample was calculated relative to the corresponding nonirradiated samples. For functional stability, mAb-CNTs, prepared as described above, were suspended in 0.1 ml of mouse serum (Sigma) and incubated at 37°C for 0–72 h. At each time point, the suspension was washed with ice-cold PBS, and the pellet was resuspended in 40 μl of PBS. The ablation of mAb-CNT-coated Daudi cells with NIR light was tested as described above.

Statistics. Data were analyzed by using Student's *t* test. Values are given as mean $\pm$ SD. $P < 0.05$ was considered statistically significant.

ACKNOWLEDGMENTS. We thank Dr. Gregg R. Dieckmann (University of Texas, Dallas) for use of the sonicator and centrifuge; Hadi N. Yehia for help during the initial stages of the project; Vicky Poenitzsch for assistance with the AFM images; Kate Walker, Meredith Daigrepont, and Jonathan Belew for assistance with elemental analyses; and Drs. Peter Wilk, Robert Stirbl, Jimmy Xu, and Malcolm Snead for unwavering support, ideas, and interactions. This work was supported by The Cancer Immunobiology Center, University of Texas Southwestern Medical Center (E.S.V., R.M., and P.C.), Robert A. Welch Foundation Grants AT-1364 (to P.P.) AT-1326 (to I.H.M.), the Department of Defense (to E.S.V. and R.K.D.) and the Center for Applied Biology at the University of Texas, Dallas. N.S.Z. and A.D.-E.S. were summer students supported by the Summer Undergraduate Research Fellowship program at the University of Texas Southwestern Medical Center.

1. Gottesman MM, Fojo T, Bates SE (2002) Multidrug resistance in cancer: Role of ATP-dependent transporters. *Nat Rev Cancer* 2:48–58.
2. Weiner LM, Adams GP (2000) New approaches to antibody therapy. *Oncogene* 19:6144–6151.
3. von Mehren AG, Weiner LM (2003) Monoclonal antibody therapy for cancer. *Annu Rev Med* 54:343–369.
4. Bross PF, *et al.* (2001) Approval summary: Gemtuzumab ozogamicin in relapsed acute myeloid leukemia. *Clin Cancer Res* 7:1490–1496.
5. Sharkey RM, Burton J, Goldenberg DM (2005) Radioimmunotherapy of non-Hodgkin's lymphoma: A critical appraisal. *Exp Rev Clin Immunol* 1:47–62.
6. Ghetie MA, *et al.* (1996) Combination immunotoxin treatment and chemotherapy in SCID mice with advanced, disseminated Daudi lymphoma. *Int J Cancer* 68:93–96.
7. Wei BR, Ghetie MA, Vitetta ES (2000) The combined use of an immunotoxin and a radioimmunoconjugate to treat disseminated human B-cell lymphoma in immunodeficient mice. *Clin Cancer Res* 6:631–642.
8. Spiridon CI, *et al.* (2002) Targeting multiple Her-2 epitopes with monoclonal antibodies results in improved antigrowth activity of a human breast cancer cell line *in vitro* and *in vivo*. *Clin Cancer Res* 8:1720–1730.
9. Coleman EJ, Brooks KJ, Smallshaw JE, Vitetta ES (2006) The Fc portion of UV3, an anti-CD54 monoclonal antibody, is critical for its antitumor activity in SCID mice with human multiple myeloma or lymphoma cell lines. *J Immunother* 29:489–498.
10. Vitetta ES, *et al.* (1991) A phase I immunotoxin trial in patients with B cell lymphoma. *Cancer Res* 51:4052–4058.
11. Amlot PL, *et al.* (1993) A phase I study of an anti-CD22 deglycosylated ricin A chain immunotoxin in the treatment of B cell lymphomas resistant to conventional therapy. *Blood* 82:2624–2633.
12. Sausville EA, *et al.* (1995) Continuous infusion of the anti-CD22 immunotoxin, IgG-RFB4-SMPT-dgA in patients with B cell lymphoma: A phase I study. *Blood* 85:3457–3465.
13. Stone M, *et al.* (1996) A phase I study of bolus vs. continuous infusion of the anti-CD19 immunotoxin, IgG-HD37-dgA in patients with B cell lymphoma. *Blood* 88:1188–1197.

14. Engert A, *et al.* (1997) A phase I study of an anti-CD25 ricin A-chain immunotoxin (RFT5-SMPT-dgA) in patients with refractory Hodgkin's lymphoma. *Blood* 89:403–410.
15. Schnell R, *et al.* (2002) A phase I study with an anti-CD30 ricin A-chain immuntoxin (Ki-4.dgA) in patients with refractory CD30+ Hodgkin's and non-Hodgkin's lymphoma. *Clin Cancer Res* 8:1779–1786.
16. Falk MH, Issels RD (2001) Hyperthermia in oncology. *Int J Hyperthermia* 17:1–18.
17. Wust P, *et al.* (2002) Hyperthermia in combined treatment of cancer. *Lancet Oncol* 3:487–497.
18. Cherukuri P, *et al.* (2006) Mammalian pharmacokinetics of carbon nanotubes using intrinsic near-infrared fluorescence. *Proc Natl Acad Sci USA* 103:18882–18886.
19. Liu Z, *et al.* (2007) *In vivo* biodistribution and highly efficient tumor targeting of carbon nanotubes in mice. *Nat Nanotechnol* 2:47–52.
20. Liu Z, *et al.* (2008) Circulation and long-term fate of functionalized, biocompatible single-walled carbon nanotubes in mice probed by Raman spectroscopy. *Proc Natl Acad Sci USA* 105:1410–1415.
21. Gobin AM, *et al.* (2007) Near-infrared resonant nanoshells for combined optical imaging and photothermal cancer therapy. *Nano Lett* 7:1929–1934.
22. Loo C, Lowery A, Halas N, West J, Drezek R (2005) Immunotargeted nanoshells for integrated cancer imaging and therapy. *Nano Lett* 5:709–711.
23. Huang X, El-Sayed IH, Qian W, El-Sayed MA (2006) Cancer cell imaging and photothermal therapy in the near-infrared region by using gold nanorods. *J Am Chem Soc* 128:2115–2120.
24. Hirsch LR, *et al.* (2003) Nanoshell-mediated near-infrared thermal therapy of tumors under magnetic resonance guidance. *Proc Natl Acad Sci USA* 100:13549–13554.
25. Kam NW, O'Connell M, Wisdom JA, Dai H (2005) Carbon nanotubes as multifunctional biological transporters and near-infrared agents for selective cancer cell destruction. *Proc Natl Acad Sci USA* 102:11600–11605.
26. Shao N, Lu S, Wickstrom E, Panchapakesan B (2007) Integrated molecular targeting of IGF1R and Her2 surface receptors and destruction of breast cancer cells using single-wall carbon nanotubes. *Nanotechnology* 18:315101–315109.
27. Weissleder R (2001) A clearer vision for *in vivo* imaging. *Nat Biotechnol* 19:316–317.
28. McDevitt MR, *et al.* (2007) Tumor targeting with antibody-functionalized, radiolabeled carbon nanotubes. *J Nucl Med* 48:1180–1189.
29. Liu Z, Sun X, Nakayama-Ratchford N, Dai H (2007) Supramolecular chemistry on water-soluble carbon nanotubes for drug loading and delivery. *ACS Nano* 1:50–56.
30. Welsher K, Liu Z, Daranciang D, Dai H (2008) Selective probing and imaging of cells with single-walled carbon nanotubes as near-infrared fluorescent molecules. *Nano Lett* 8:586–590.
31. Marches R, *et al.* (1995) Tumor dormancy and cell signaling III. Role of hypercross-linking of IgM and CD40 on the induction of cell cycle arrest and apoptosis in lymphoma cells. *Ther Immunol* 2:125–136.
32. Zorbas V, *et al.* (2004) Preparation and characterization of individual peptide-wrapped single-walled carbon nanotubes. *J Am Chem Soc I* 126:7222–7227.
33. Chin S-F, *et al.* (2007) Amphiphilic helical peptide enhances the uptake of single-walled carbon nanotubes by living cells. *Exp Biol Med* 232:1236–1244.
34. Schnyder A, Krahenbuhl S, Torok M, Drewe J. Huwyler J (2004) Targeting of skeletal muscle *in vitro* using biotinylated immunoliposomes. *Biochem J* 377:61–67.

Int. J. Cancer: **000,** 000–000 (2009)

Specific thermal ablation of tumor cells using single-walled carbon nanotubes targeted by covalently-coupled monoclonal antibodies

Radu Marches[1], Pavitra Chakravarty[1], Inga H. Musselman[2,3], Pooja Bajaj[2], Robert N. Azad[2], Paul Pantano[2,3], Rockford K. Draper[2,3,4] and Ellen S. Vitetta[1,5,6]*

[1]*The Cancer Immunobiology Center, University of Texas Southwestern Medical Center, Dallas, TX*
[2]*Department of Chemistry, The University of Texas at Dallas, Richardson, TX*
[3]*The Alan G. MacDiarmid NanoTech Institute, The University of Texas at Dallas, Richardson, TX*
[4]*Department of Molecular and Cell Biology, The University of Texas at Dallas, Richardson, TX*
[5]*Department of Microbiology, University of Texas Southwestern Medical Center, Dallas, TX*
[6]*Department of Immunology, University of Texas Southwestern Medical Center, Dallas, TX*

CD22 is broadly expressed on human B cell lymphomas. Monoclonal anti-CD22 antibodies alone, or coupled to toxins, have been used to selectively target these tumors both in SCID mice with xenografted human lymphoma cell lines and in patients with B cell lymphomas. Single-walled carbon nanotubes (CNTs) attached to antibodies or peptides represent another approach to targeting cancer cells. CNTs convert absorbed near-infrared (NIR) light to heat, which can thermally ablate cells that have bound the CNTs. We have previously demonstrated that monoclonal antibodies (MAbs) *noncovalently* coupled to CNTs can specifically target and kill cells *in vitro*. Here, we describe the preparation of conjugates in which the MAbs are *covalently* conjugated to the CNTs. The specificity of both the binding and NIR-mediated killing of the tumor cells by the MAb-CNTs is demonstrated by using $CD22^+CD25^-$ Daudi cells, $CD22^-CD25^+$ phytohemagglutinin-activated normal human peripheral blood mononuclear cells, and CNTs covalently modified with either anti-CD22 or anti-CD25. We further demonstrate that the stability and specificity of the MAb-CNT conjugates are preserved following incubation in either sodium dodecyl sulfate or mouse serum, indicating that they should be stable for *in vivo* use.

Key words: Single-walled carbon nanotube; monoclonal antibody; near-infrared thermal ablation; cancer therapy

The ability of carbon nanotubes (CNTs) to absorb near-infrared (NIR) radiation (700–1100 nm) and convert it into heat provides an opportunity to create a new generation of immunoconjugates for cancer photo-therapy.[1–3] In brief, NIR light can effectively and safely penetrate normal tissue and ablate any cells to which the CNTs are attached. The use of NIR-resonant nanostructures, including gold nanoshells, gold nanorods, and CNTs, to thermally ablate cancer cells is being explored by several groups.[2,4–8] In addition to its intrinsic lethal effects, hyperthermia has been clinically used in the treatment of solid tumors because it can enhance the efficiency of chemo- or radiotherapy.[9,10] Hyperthermia also preferentially increases the permeability of tumor vasculature compared to normal vasculature, which can enhance the delivery of drugs to tumors.

One critical aspect concerning the therapeutic use of CNTs is their tissue biodistribution, blood circulation time, and toxicity. Recent pharmacokinetic (PK) studies in experimental animals have reported that CNTs functionalized with non-covalent and covalent dispersants have a blood circulation half-lives ($t_{1/2}$) ranging from 30 min to 3 hr, in mice[3,11] or 1 hr, in rabbits.[12] Similar studies reported that the level of CNTs in mice was reduced to 5% of the injected dose per gram (ID/g) within 1.2 to 5 hr, in case of noncovalently functionalized CNTs[13] or to less than 3% ID/g, in case of covalently functionalized CNTs.[14] Of note, none of these studies reported apparent toxic effects during the observation time. Another critical aspect for the selective CNT-mediated thermal ablation of cells is the physiological stability of the linkage between the targeting moieties and the CNTs. To date, the targeting of CNTs to tumor cells for NIR-mediated killing has been accomplished by non-covalently coating CNTs with cell-binding ligands such as peptides or monoclonal antibodies (MAbs).[2,8,15,16] We, too, have previously generated targeted CNTs consisting of Neutravidin (NA)-conjugated MAbs attached to a biotinylated (B) polymer that non-covalently coated the CNTs.[17] These conjugates were shown to selectively bind to and thermally ablate tumor cells following the exposure of the targeted cells to NIR radiation. The use of B-CNTs and NA-MAbs allowed us to "assemble" the targeted CNTs using any targeting MAb that could be bound to NA. However, there is a potential limiting factor in applying this strategy in animals because non-covalently attached molecules might be displaced by other macromolecules in biological fluids, resulting in the disassociation of the targeting moiety from the NIR-absorbing nanostructure.[12] For this reason, in the present study, we tested an alternative strategy where the targeting molecule was covalently coupled to the CNTs. In this approach, amide bonds are formed between free amines on the MAbs and carboxylic acid groups on the chemically oxidized CNTs.[18–21] A potential disadvantage is that covalent modification of CNTs may interfere with the electronic and optical properties of the CNTs. However, even carboxylated CNTs retain significant background absorption in the NIR region which may still support NIR-mediated photothermal therapy.[22,23] An advantage of using MAbs for targeting is their superior circulation time compared to that of CNTs. Thus, the $t_{1/2}$ of murine MAbs in normal mice ranges from 121 hr (IgG_{2b}) to 228 hr (IgG_3), in particular, 197 hr for the targeting MAbs used in this study (IgG_1),[24] although, in tumor-bearing mice the presence of the tumor might act as a sink for the injected MAbs and decrease their $t_{1/2}$. The attachment of MAbs to CNTs might, therefore, improve the $t_{1/2}$ of the CNTs and increase the chance to target the tumor.

The aim of this study was to design and prepare CNTs covalently attached to anti-CD22 antibodies for the selective thermal ablation of human B lymphoma cells. Herein, we describe the physical properties of these CNT constructs, their selective binding to tumor cells, and the NIR light-induced thermal ablation of the targeted tumor cells *in vitro*.

Material and methods

Antibodies and other reagents

Mouse IgG_1 anti-human CD22 (RFB4)[25] and mouse IgG_1 anti-human CD25 (RFT5)[26] were prepared and purified in our labora-

Abbreviations: AFM, atomic force microscopy; CNT, single-walled carbon nanotubes; EGFP, enhanced green fluorescent protein; MAb, monoclonal antibody; NIR, near-infrared; PBMC, peripheral blood mononuclear cells; PHA, phytohemagglutinin.

Grant sponsor: The Cancer Immunobiology Center, DOD; Grant number: W81XWH-08-2-0004; Grant sponsor: The Norman Hackerman Texas Advanced Research (Biological Sciences) Program; Grant number: 009741-0005-2007; Grant sponsor: The Robert A. Welch Foundation; Grant numbers: AT-1364, AT-1326.

***Correspondence to:** Cancer Immunobiology Center, University of Texas Southwestern Medical Center, 6000 Harry Hines Blvd., Dallas, TX 75390-8576, USA. E-mail: ellen.vitetta@utsouthwestern.edu

Received 23 January 2009; Accepted after revision 9 June 2009
DOI 10.1002/ijc.24659
Published online 17 June 2009 in Wiley InterScience (www.interscience.wiley.com).

tory. Carboxyl-functionalized CNTs (purity ≈ 80–90%, 3–6 atomic% carboxylic acid, and an average diameter of individual CNTs 1.4 ± 0.1 nm, as per manufacturer's specifications) were purchased from Sigma-Aldrich (St. Louis, MO). 1-Ethyl-3-[3-dimethylaminopropyl] carbodiimide hydrochloride (EDC) and sulfo *N*-hydroxysuccinimide (NHS) were purchased from Pierce Endogen (Rockford, IL). Enhanced green fluorescent protein (EGFP) was purchased from BioVision (Mountain View, CA). Fluorescein isothiocyanate (FITC)-labeled goat anti-mouse IgG (GAMIg) was purchased from Invitrogen (Carlsbad, CA).

Cell culture

Daudi cells (human Burkitt's lymphoma cell line, American Type Culture Collection, Manassas, VA) were cultured in RPMI-1640 medium (Sigma) containing 1% antibiotic-antimycotic mixture (penicillin/streptomycin/amphotericin B) (Sigma), 10% heat-inactivated fetal calf serum (HyClone, Logan, UT), and 2 mM L-glutamine (Sigma) (complete medium). Peripheral blood mononuclear cells (PBMCs) from normal healthy donors were isolated from the fresh heparinized blood by Ficoll-Paque PLUS (GE Healthcare, Piscataway, NJ) density gradient centrifugation. Normal activated $CD25^+$ cells were generated by culturing the PBMCs for 72 hr at 1×10^6 cells/ml in complete medium supplemented with 5 μg/ml phytohemagglutinin (PHA; Sigma). We chose to use activated PBMCs since we could not identify an established cell line that expressed high levels of CD25, one of our 2 target antigens.

Preparation of MAb-CNT conjugates

Carboxyl-functionalized CNTs (0.5 mg) were dispersed in 1 ml of 0.1 M 2-[*N*-morpholino]ethane sulfonic acid (MES) buffer, pH 4.5 with 0.2% Tween 20 (activation buffer) by sonication with a 2-mm probe tip connected to a Branson Sonifier 250 (VWR, West Chester, PA) for 5 min at a power level of 10 W, with the sample immersed in ice. The mixture was then centrifuged at 16,000*g* for 15 min to remove undispersed material. The supernatant containing the dispersed CNTs was recovered. The carboxyl groups on the CNTs were activated by incubation for 30 min at room temperature in 1 ml of 0.1 M MES buffer/0.2% Tween 20 containing 2 mM EDC and 5 mM NHS. The excess reagents were removed by centrifugation in an Amicon Ultra-4 centrifugal filter unit (Millipore, MA) and the CNTs were washed and filtered twice with binding buffer (0.1 M phosphate buffered saline [PBS], pH 7.2 with 0.2% Tween 20). The activated CNTs were recovered in 1 ml binding buffer and reacted with 10 mg IgG anti-CD22 (RFB4) or IgG anti-CD25 (RFT5) MAb for 2 hr at room temperature by gentle rocking. Control experiments were carried out using a mixture of MAb and non-activated, carboxyl-functionalized CNTs. In both cases, the unreacted MAbs were removed by centrifugation at 16,000*g* for 30 min. The supernatant containing unreacted MAb was discarded, and the pellet was resuspended and washed twice with 1 ml aliquots of PBS (10 mM, pH 7.4). After each wash, the CNTs were briefly sonicated for 10 sec at a power level of 10 W. The amount of CNT-bound MAbs was quantified using the bicinchoninic acid (BCA) protein assay (Pierce Endogen) and the CNT concentration was determined from the linear absorbance at 808 nm observed over the concentration range of 0.2–60 μg CNT/ml, as determined using a DU-730 Beckman-Coulter UV–Vis spectrophotometer (Fullerton, CA).[16] To *directly* visualize the binding of MAb-CNTs to target cells, CNTs were conjugated to both MAb and EGFP. For the coupling reaction, 10 mg MAb and 100 μg EGFP were reacted with activated CNTs as mentioned above. The binding of these fluorescent conjugates to target cells was analyzed by both flow cytometry and fluorescent microscopy. The stability of the conjugates was analyzed by electrophoresis on 7.5% sodium dodecyl sulfate-polyacrylamide gels (SDS-PAGE). The presence of any dissociated protein was detected by staining with SimplyBlue SafeStain (Invitrogen, Carlsbad, CA).

MAb-CNT analyses

Atomic force microscopy (AFM) images (2.0 × 2.0 μm for diameter analyses and 5.0 × 5.0 μm for length analyses) of carboxylated-CNTs and RFB4-coupled CNTs were acquired in air under ambient conditions using a Digital Instruments Nanoscope III Multimode scanning probe microscope operated in the TappingMode.[27] The instrument conditions included a reduced Z-limit (100–200 V) and cantilevers with average force constants and resonant frequencies of 5.0 N/m and 180 kHz, respectively. For carboxylated-CNTs and RFB4-coupled CNTs, 20 μl of the dispersion was spun cast on to freshly cleaved mica at 3500 rpm for 30 sec. The samples were dried in a desiccator overnight prior to imaging.

Background-corrected UV–Vis–NIR absorption spectra of carboxylated-CNT and MAb-CNT samples were obtained between 400 and 1100 nm using a dual-beam Lambda 900 UV–Vis–NIR spectrophotometer (PerkinElmer, Waltham, MA) with a 0.48 sec integration time at a scan speed of 125 nm/min. Raman spectra were acquired using a LabRAM HR high resolution confocal Raman microscope system (Horiba Jobin Yvon, Edison, NJ) as described earlier.[28] The laser excitation was provided by a 785 nm diode laser (Renishaw, UK) operating at 300 mW. Wavenumber calibration was performed using the 520.5 cm^{-1} line of a silicon wafer and the spectral resolution was ~1 cm^{-1}. Using a 10× objective, Raman spectra were acquired from carboxylated-CNT and MAb-CNT dispersions contained in 35 mm polylysine-coated glass bottom "imaging" dishes (MatTek, Ashland, MA).

The binding of MAb-CNTs to target cells

A million Daudi cells or PHA-activated PBMCs (>95% $CD25^+$ cells) were incubated with the MAb-CNTs (containing 1 μg CNT) for 15 min at 4°C in PBS and then washed twice with cold 10 mM PBS, pH 7.4. Cells were subsequently incubated with FITC-GAMIg for 15 min at 4°C and then washed twice with cold PBS. The cells were then resuspended in 0.5 ml of PBS and the bound fluorescence was analyzed on a FACScan (Becton Dickinson, San Jose, CA). Direct immunofluorescence staining was performed with EGFP-conjugated RFB4-CNTs for 15 min on ice, and washed with cold PBS. Half of the cells were analyzed by flow cytometry. The other half were allowed to adhere to poly-L-lysine-coated slides (Sigma) at room temperature for 20 min and then were fixed with 3% paraformaldehyde for 10 min. The slides were washed twice with PBS, rinsed with distilled water, air-dried, and mounted with Vectashield mounting medium (Vector Laboratories, Burlingham, CA) containing 4′,6-diamidino-2-phenylindole (DAPI) as counterstain. The slides were examined under a fluorescence microscope (Axiophot, Zeiss, Germany) under a 63× objective using single-pass filters for FITC (green) and DAPI (blue) or a dual-pass green/blue filter set.

To determine the amount of RFB4-CNTs necessary to saturate Daudi cells, 10^6 cells were incubated with increasing amounts of MAb-CNTs for 15 min at 4°C in PBS, washed two times with cold PBS, and stained with FITC-GAMIg. The amount of MAb-CNTs bound to cells was determined by flow cytometry.

NIR-mediated thermal ablation of cells targeted with MAb-CNTs

A million cells were incubated with MAb-CNTs containing 3 μg CNTs in PBS for 15 min at 4°C. Cells were washed 3 times with cold PBS, and then 10^5 cells were dispensed in triplicate wells in a 96-well plate in 200 μl complete medium. The cells were immediately exposed to continuous NIR light using a FAP-Sys-30W 805-811 nm laser system (Coherent, Santa Clara, CA) for 4 min at 9.5 W/cm^2. Cell death was assessed by pulsing the cells for the next 12 hr with 1 μCi [^{3}H]-Thymidine/well (GE Healthcare Bio-Sciences, Piscataway, NJ) and the incorporated radioactivity was measured by liquid scintillation counting. The percent incorporated radioactivity for each sample was calculated relative to the corresponding nonirradiated samples.

Statistics

Data were analyzed by using Student's *t* test. Values are given as mean ± SD. A p value <0.05 was considered statistically significant.

Results

Preparation and analysis of the MAb-CNT conjugates

RFB4-CNTs and RFT5-CNTs were prepared by first activating ~0.5 mg of carboxylated CNTs with EDC and NHS. After the excess reagents and urea by-product were removed, the NHS ester-derivatized CNT suspension (~0. 25 mg CNTs) was transferred in 0.1 M PBS with 0.2% Tween 20 and coupled to RFB4 or RFT5 for 1 hr at room temperature, which should lead to the formation of amide bonds between primary amines on the MAbs and the NHS-functionalized CNTs. To rule out the potential noncovalent attachment of IgG to CNTs, the nonactivated, carboxyl-functionalized CNTs were incubated with MAbs under the same conditions (control). Finally, these conjugates were transferred to 10 mM PBS by 3 cycles of centrifugation to remove free Tween 20 and unreacted MAbs from the solution. After every wash, the CNT pellet was resuspended and sonicated for a few seconds to generate a homogenous suspension with a recovery of 0.18 mg CNTs. The concentration of CNTs was calculated from the OD808 as previously described,[17] whereas bound MAb was detected using a BCA protein assay. Thus, we found 3 mg MAb/mg CNT (0.02 μmol IgG/mg CNT) in the reaction product using activated CNTs and undetectable levels of MAb in the noncovalent binding control. The solubility of such MAb-CNTs is maintained at a concentration up to 240 μg/ml. This result indicates that the binding of the MAbs to the NHS-functionalized CNTs was specific and covalent.

The dimensions of dispersed MAb-CNTs were determined using AFM. Figure 1*a* shows a representative image of the CNTs after attaching them to RFB4. The dried MAb-CNT sample showed signs of cross-linking with lengths that ranged from 0.5 to 2.0 μm with an average length of 1.0 ± 0.3 μm (number of measurements, $n = 19$). The lengths of the carboxylated-CNTs ranged from 0.2 to 1.5 μm with an average length of 0.7 ± 0.3 μm ($n = 31$) (data not shown). The diameters of the MAb-CNTs ranged from 9.0 to 20.0 nm with an average diameter of 12.3 ± 2.5 nm ($n = 20$). The diameters of the carboxylated-CNTs ranged from 2.8 to 9.0 nm with an average diameter of 5.9 ± 1.8 nm ($n = 20$), indicating a surface coating of the Tween 20 surfactant. Comparing the diameters of the carboxylated-CNTs with those of the RFB4-coupled CNTs suggests that the average 6 nM increase in diameter can be attributed to the presence of the MAb. Although AFM imaging confirmed the formation of the RFB4-CNT conjugate, the nature of the linkage could be covalent and/or noncovalent. To further investigate if the linkage was covalent, the MAb-CNTs were dispersed in SDS and electrophoresed on a 7.5% PAGE under nonreducing conditions. As shown in Figure 1*b*, no IgG in the RFB4-CNT samples entered the running gel, demonstrating that the CNT-bound IgG remained in the loading well firmly attached to CNTs. In contrast, a MAb band was detected in a control sample that contained a mixture of equivalent amounts of MAb and carboxylated-CNTs that were not activated with EDC and NHS. In summary, the combined evidence supports that the linkage between the MAbs and the CNTs was covalent.

For their use in photothermal therapy, we next determined if the optical properties and structure of the MAb-CNT conjugate were affected by the covalent coupling. First, the UV–Vis–NIR absorption spectrum of MAb-CNTs (Fig. 1*c*) closely matched that of the starting material (*i.e.*, carboxylated-CNTs dispersed in aqueous MES; data not shown) in that both displayed a large pie-plasmon absorption band. Next, MAb-CNTs were analyzed using microprobe Raman spectroscopy (Fig. 1*d*). The G-band, observed at ~1590 cm^{-1} in the Raman spectrum of the RFB4-CNT conjugate, exhibited a G^-/G^+ line shape that is characteristic of single-walled CNTs, and that was identical to the starting material. Interestingly, the ratio of the areas of the D-band (at ~1310 cm^{-1}) for MAb-CNTs was more than 2-fold greater than that observed for the original dispersed carboxylated-CNT material. Since the quality of CNT samples is often evaluated using this ratio, this indicates that the MAb-to-CNT synthetic procedure additionally purified. This result is in agreement with our previous results in which >99% of metal impurities found in the as-received CNT powder were removed by the sonication and centrifugation steps.[17,28] The detection of single-walled CNT resonances in the radial breathing mode (RBM) region of Raman spectra acquired from MAb-CNTs and the starting material (data not shown), combined with AFM images and optical spectroscopy experiments, provide strong evidence for the presence of CNTs in our immunoconjugate preparations.

Specific binding of MAb-CNTs to cells

For imaging purposes, we prepared CNTs coupled to both MAbs and EGFP, and then determined the ability of these MAb-CNT conjugates to bind to $antigen^+$ but not $antigen^-$ target cells using flow cytometry. The cell-bound MAb-CNTs were detected using FITC-GAMIg. We found that RFB4-CNTs bound well to Daudi cells, whereas the RFT5-CNTs (negative control) bound poorly (Figs. 2*a* and 2*b*). Conversely, RFT5-CNTs and RFT5 bound equally well to $CD22^-CD25^+$ PHA-activated PBMCs (95% $CD25^+$ cells), whereas the negative control conjugate, RFB4-CNT, did not (Figs. 2*a* and 2*b*). Additional experiments using nonactivated, carboxyl-functionalized CNTs incubated with targeting antibody (control) indicated no detectable binding to cells (data not shown). This result indicates that CNTs are free of adsorbed MAb. Taken together, these results demonstrate that the MAb-CNTs bind specifically to antigen-expressing cells. The binding to target cells was confirmed by flow cytometric analysis of the CNTs cocoupled to targeting MAb and EGFP (Fig. 2*c*, left panel) and fluorescence microscopy (Fig. 2*c*, right panel).

In separate experiments, we detected saturation levels of MAb-CNTs on Daudi cells by adding from 0.25 to 4 μg CNTs, containing an equivalent of 0.75–12 μg bound RFB4 (Fig. 3). The results indicate that saturation is achieved at 0.25 μg CNTs.

The stability of the MAb-CNT conjugate was established by incubating RFB4-CNTs (1 μg CNTs) in 500 μl mouse serum at 37°C for up to 24 hr. At the end of incubation, the RFB4-CNTs were recovered by centrifugation and then tested for their ability to bind to $CD22^+$ Daudi cells, using RFT5-CNT as the negative control. As shown in Figure 4, we found that their binding was not diminished.

Thermal ablation of target cells

We next determined whether cells targeted by the MAb-CNTs could be thermally ablated following exposure to NIR light. Cells were incubated with the MAb-CNTs in PBS for 15 min and, after the excess unbound CNTs were removed, cells were suspended in culture medium and dispensed into 96-well plates. The cells in the plate were exposed to an 808 nm laser (9.5 W/cm^2) for 4 min and pulsed for the next 12 hr with 1 μCi [^{3}H]-Thymidine to assess their proliferative capacity, which is our standard method to measure cell viability. When compared with the nonbinding control RFT5-CNTs, the viability of the RFB4-CNT-treated Daudi cells was significantly ($p < 0.01$) reduced following exposure to NIR light (Fig. 5*a*). Conversely, when activated PBMCs were used as target cells, RFT5-CNTs, but not the control RFB4-CNTs, killed the cells following exposure to NIR light (Fig. 5*b*). The selective photothermal damage responsible for the inhibition of proliferation was confirmed under light microscopy as the loss of morphological integrity in Daudi cells pretreated with RFB4-CNT (Fig. 6*b*) but not in untreated or control treated cells (Figs. 6*a* and 6*c*). The proliferation of cells treated with MAb-CNTs in the absence of NIR was significantly lower ($p < 0.05$) than the proliferation of

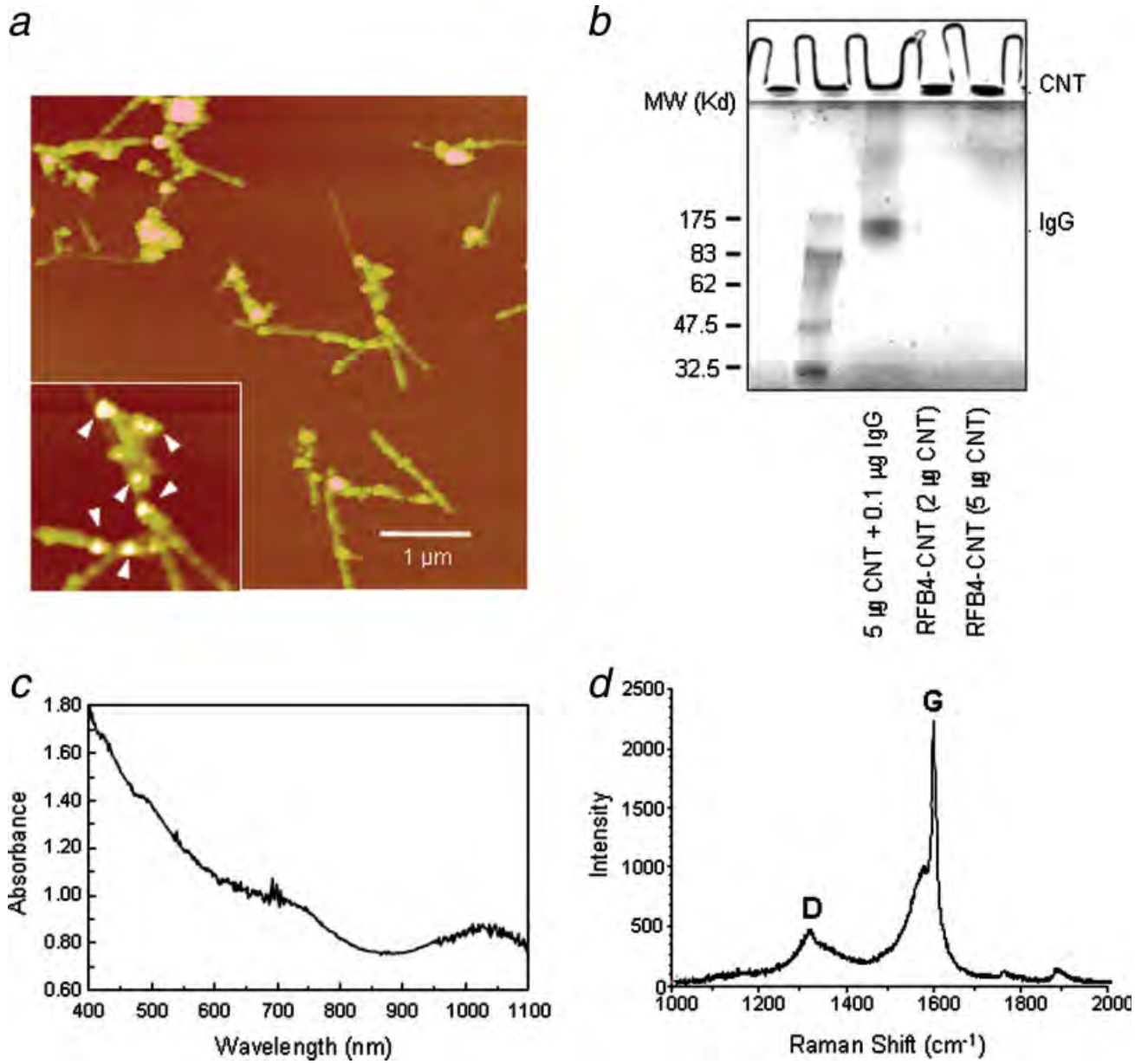

Figure 1 – Physical and optical properties of RFB4-CNTs. (*a*) AFM image showing CNTs coated with MAbs. The enlarged inset shows where the MAbs are presumably attached to the CNTs (white arrowheads). This AFM image is representative of AFM images acquired from two unique MAb-CNT dispersions. (*b*) Stability of RFB4-CNTs. Purified RFB4-CNTs or a mixture of carboxylated CNTs and RFB4 (control) were subjected to SDS-PAGE. Samples containing 2 or 5 μg CNTs were loaded on the gel. The stacking gel shows the accumulation of CNTs whereas dissociated IgG migrated into the gel. The presence of dissociated protein was detected by staining with SimplyBlue SafeStain. (*c*) Background corrected UV–Vis–NIR absorption spectrum of RFB4-CNTs. (*d*) Representative Raman spectrum (785-nm laser excitation) of RFB4-CNTs (*i.e.*, carboxylated-CNTs after covalent coupling of MAb) showing the D-band at ~1310 cm^{-1} and the G-band at ~1590 cm^{-1}. [Color figure can be viewed in the online issue, which is available at www.interscience.wiley.com.]

untreated cells (Figs. 5*a* and 5*b*). This may be due to an extensive cross-linking of the target antigen by the CNT-bound MAbs and subsequent signaling of growth arrest and/or apoptosis. This possibility is supported by the observation that cells undergo massive clustering. Indeed, Daudi cells pretreated with RFB4-CNTs formed "tissue-like" structure of aggregates with large contact areas after 12 hr of incubation (Fig. 6*e*). In contrast, no aggregates (Fig. 6*f*) and no inhibition of cell proliferation (Fig. 5*a*) occurred when cells were treated with control RFT5-CNTs. These indicate that the homotypic adhesion and the concurrent inhibitory effect are receptor-dependent and do not involve any CNT-mediated nonspecific adhesion. These experiments demonstrate that the binding of the MAb-CNTs to their target cells leads to their specific ablation following exposure to NIR light and the overall inhibitory effect is further enhanced by receptor hyper-crosslinking.

Discussion

CNTs have attracted considerable attention due to their remarkable structural, electrical and mechanical properties. Their ability

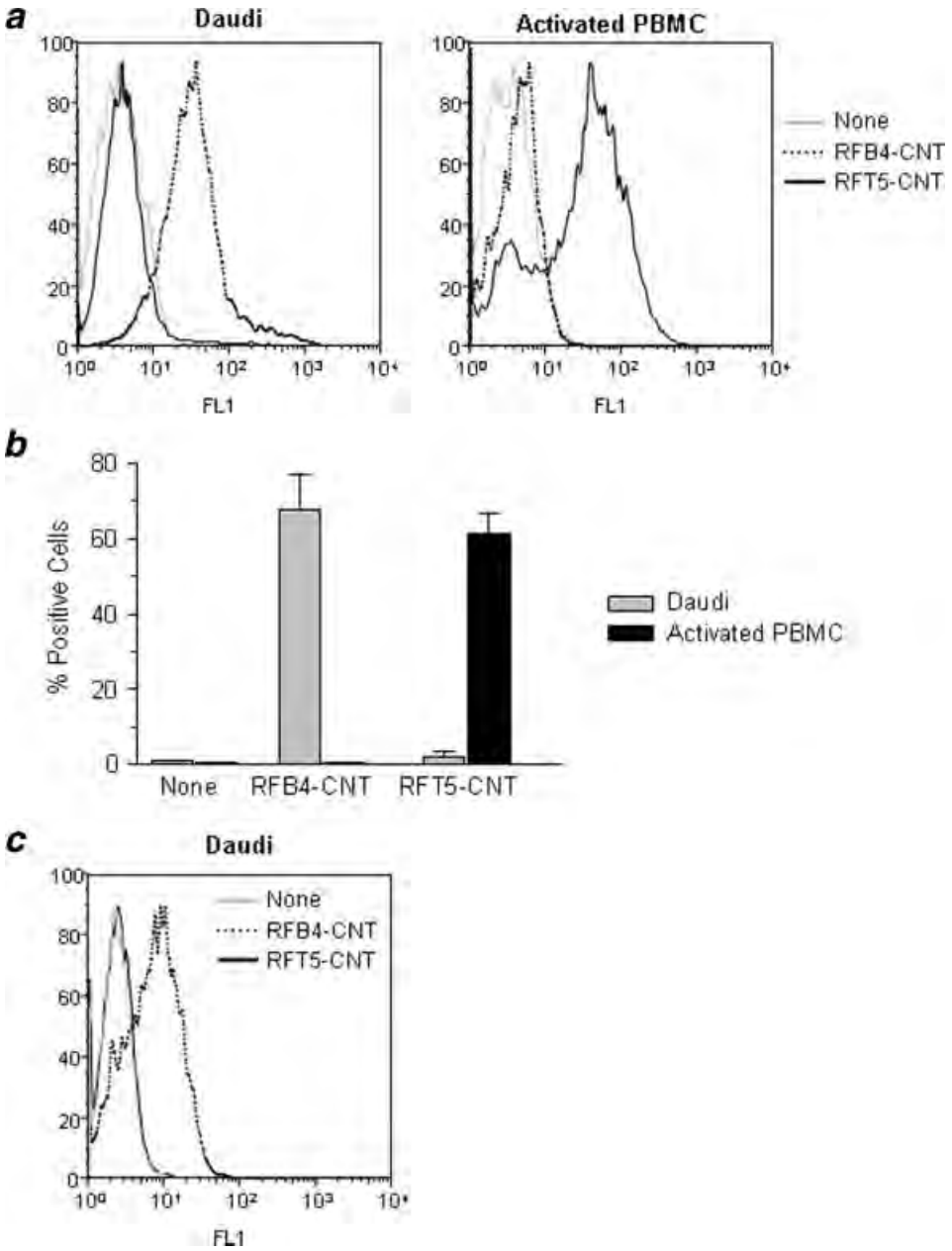

FIGURE 2 – Specific binding of MAb-CNTs to target cells. (*a*) Daudi cells or PHA-activated human PBMCs were stained with either RFB4-CNTs or RFT5-CNTs (1 μg CNT) followed by FITC-GAMIg and cells were analyzed by flow cytometry. Histograms showing the staining with RFB4-CNTs (blue line) and RFT5-CNTs (red line) are overlaid on the ones corresponding to unstained cells (grey line) in each panel. (*b*) The results of three independent binding experiments are presented as means of % positive cells ± SD. The binding of MAb-CNTs to target *vs*. non-target cells was highly specific ($p < 0.01$) (*c*) The binding of RFB4-CNTs to Daudi cells was confirmed by direct fluorescence using CNTs coconjugated to RFB4 and EGFP. Cell binding was revealed by flow-cytometry (shown) and fluorescence microscopy (data not shown) as described in the "Material and methods".

to absorb NIR light and convert it into heat can be exploited for killing tumor cells. The critical challenge is to selectively deliver heat to tumor cells and not to normal tissues. In our previous study,[17] as well as in published reports by others,[2,8] the selective NIR photothermal ablation of cells has been achieved by using CNTs *noncovalently* attached to targeting ligands. A concern of using noncovalently attached targeting ligands is that the targeting ligand might dissociate from the CNTs *in vivo*. Linkage stability and specific targeting can be achieved by covalent attachment of the targeting moiety to CNTs. Thus, McDevitt *et al*.[14] used an ylide cycloaddition synthetic route to covalently couple an anti-CD20 MAb to CNTs. However, the objective of their study was to deliver radionuclides to cells, not to ablate cells with NIR light.

Herein, we describe the use of MAbs covalently attached to CNTs for targeting and NIR photothermal ablation of human B lymphoma cells *in vitro*. The major findings to emerge from this study are: (*i*) The MAbs were stably attached to the CNTs and the ~12 nm diameter × ~1 μm long MAb-CNTs were well dispersed; (*ii*) The MAb-CNT conjugates were chemically stable and free from noncovalently attached MAb; (*iii*) The conjugates bound specifically to target cells and the binding remained specific even

after the MAb-CNTs were incubated in mouse serum and (*iv*) specifically targeted cells were thermally ablated following exposure to RFB4-coupled CNTs and NIR light.

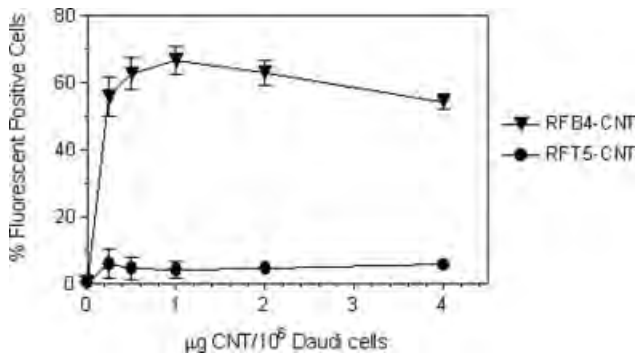

Figure 3 – Saturation of Daudi cells with RFB4-CNTs. A million cells were incubated on ice with RFB4-CNTs or RFT5-CNTs in concentrations ranging from 0.25 to 4 µg in a total volume of 200 µl of PBS. After 3 washes with PBS cells were incubated with FITC-GAMIg, washed and analyzed by flow cytometry. The results of three independent binding experiments are presented as means of % positive cells ± SD.

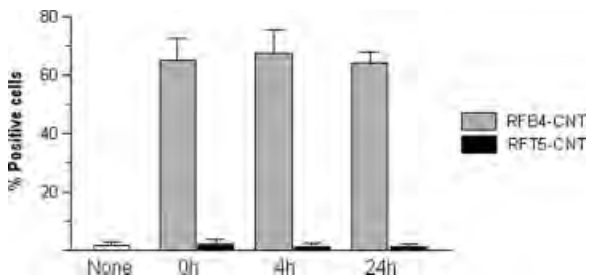

Figure 4 – Binding stability of RFB4-CNTs. The stability of the RFB4-CNTs *in vitro* was determined by incubating them (1 µg CNT) in mouse serum at 37°C for 0, 4 and 24 hr. At each time point, the RFB4-CNTs were recovered by centrifugation, washed with PBS and incubated with Daudi cells and the positive binding detected by flow cytometry. Data represent mean ± S.D. of at least three independent experiments.

The chemical and binding stability of the MAb-CNT conjugates, as well as their stability in serum, are important features for their use *in vivo*. However, one of the major concerns with the covalent attachment of targeting ligands is that chemical stability can increase at the expense of photothermal efficacy due to the defects in the sp^2 hybridization of the CNTs induced by chemical functionalization.[29] However, we found that chemical coupling of the MAb to CNT did not destroy the optical properties critical for the conversion of NIR light into heat. Indeed, the results of this study and of our previous work[17] indicate that there were no significant differences in the selectivity and killing efficiencies between noncovalently and covalently conjugates, using identical targeting MAbs, MAb-CNTs of similar dimensions, and essentially identical experimental conditions. Therefore, since both constructs thermally ablated target cells with the same efficiency and selectivity, the data indicate that the pie-plasmon of oxidized-CNTs is capable of absorbing NIR light and converting it to heat under these conditions.

The potential cytotoxicity of CNTs has been of concern for their use in animals. One of the major challenges is to minimize their nonspecific interaction with serum proteins and/or cells and tissues and increase their half-life in the circulation. In previous reports, this was achieved by coating CNTs with biocompatible compounds, such as hydrophilic uncharged polymers including poly-(ethylene glycol). On noncovalent functionalization, CNTs appear to be less cytotoxic than non-functionalized CNTs *in vitro*.[29–32] Short-term studies found no toxic effects of the functionalized CNTs in experimental animals[3,11,12,33] even 4 months or longer after systemic administration[13] when CNTs persisted within liver and spleen macrophages.

Relevant to our study, previous reports have indicated that increased levels of carboxyl functionalization increases CNT solubility and decreases their cytotoxicity.[34] In this report, the viability of cells cultured with nonbinding MAb-CNTs was indistinguishable from that of cells grown in the absence of CNTs. By contrast, cells cultured with targeted-CNTs did not proliferate as well due to receptor-mediated signaling of cell cycle arrest and/or cell death. This has been observed previously using cross-linking MAbs specific for different B cell surface markers and is therefore not surprising.[35,36] Regardless, this demonstrates that the CNT conjugates described in this study are biocompatible with cells *in vitro*. Importantly, when the cells were exposed to NIR light in the study reported here, specific killing was uncompromised.

Previous reports indicated that noncovalently[37–41] or covalently[42] functionalized CNTs are able to penetrate and to transport

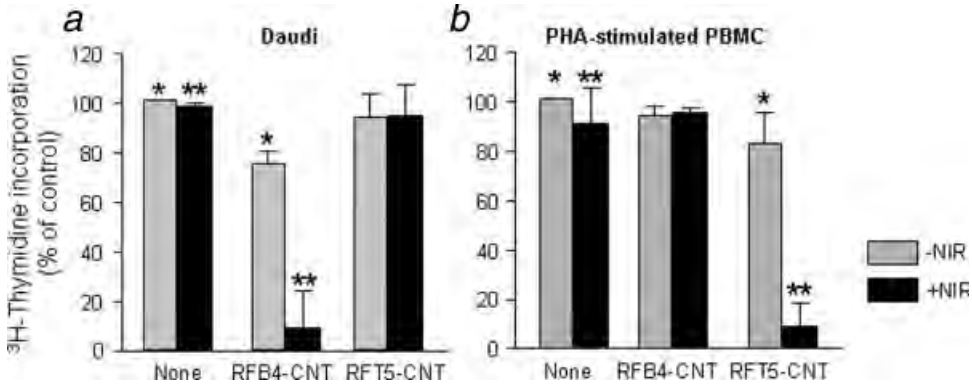

Figure 5 – Specific killing of target cells by MAb-CNTs following exposure to NIR light. A million cells were incubated with MAb-CNTs containing 3 µg CNTs in PBS for 15 min at 4°C. Cells were washed three times with ice-cold PBS, and then 10^5 cells were dispensed in triplicate wells in a 96-well plate in 200 µl complete medium. The cells were exposed to continuous NIR light for 4 min at 9.5 W/cm^2. Cell death was assessed by pulsing the cells for the next 12 hr with 1 µCi [^{3}H]-Thymidine/well and the incorporated radioactivity was measured by liquid scintillation counting. The incorporated radioactivity for each sample was calculated relative to the corresponding nonirradiated samples. (*a*) The specific killing of Daudi cells by RFB4-CNTs using RFT5-CNTs as the negative control. (*b*) The specific killing of activated PBMCs (>95% T cells) by RFT5-CNTs using RFB4-CNTs as the negative control (*$p < 0.01$; **$p < 0.05$). Data represent mean ± S.D. of at least three independent experiments.

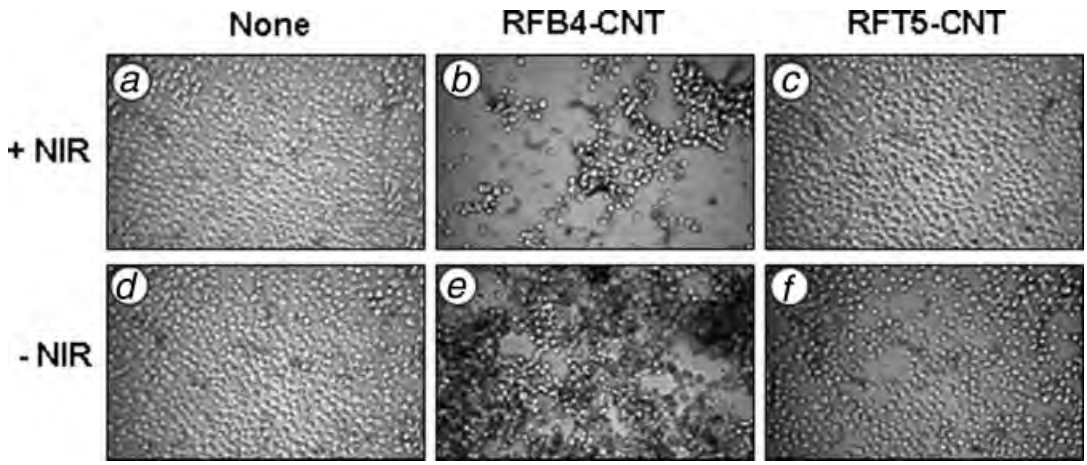

FIGURE 6 – Morphological features of Daudi cells following treatment with MAb-CNT and NIR irradiation. A million Daudi cells were incubated with or without MAb-CNTs containing 3 μg CNTs in PBS for 15 min at 4°C. Cells were washed three times with ice-cold PBS, and then 2×10^5 cells were dispensed in a 24-well plate in 400 μl complete medium. The cells were exposed or not to continuous NIR light for 4 min at 9.5 W/cm^2. Cell morphology was assessed 12 hr later by light microscopy (Magnification, ×40 in all panels).

various cargos inside mammalian cells including proteins, peptides, and nucleic acids, although the mechanism of internalization is still a matter of debate. Most of these studies depend on nonreceptor-mediated internalization of CNTs, *i.e.* pinocytosis and phagocytosis, and involve a high degree of nonspecificity. However, the major challenge for selective photothermal ablation of tumor tissues is to avoid the nonspecific binding/internalization that will cause damage to normal tissues following exposure to NIR light. The use of specific ligands including MAbs is supposed to provide selective CNT internalization *via* receptor-mediated endocytosis. Relative to the targeting MAb used in this study, reports of ours and others have shown that anti-CD22 MAbs are rapidly internalized after binding to CD22 on a variety of B-cell lines including Daudi.[43–45] This internalization capability explains, at least in part, the success achieved when CD22 has been employed as a target molecule for delivering toxins into neoplastic B-cells.[43,46] However, the anti-CD22 MAb and the attached CNT require metabolic activity to accumulate in cells because most of it remains at the cell surface after incubation at 4°C, when energy-dependent uptake ceases.[47] In this study, cell targeting and killing was achieved after a brief incubation with MAb-CNTs on ice immediately followed by NIR irradiation. This argues that the photothermal depletion under NIR light is due to MAb-CNTs on the cell surface rather than inside the cells. The magnitude of thermal damage might also depend on the cellular localization of CNTs. It is, therefore, reasonable to speculate that the extent of cellular damage will be substantially higher for the same temperature spike released by CNTs at subcellular rather than at plasma membrane level, as previously reported.[2,8] This will minimize the potential damage to adjacent normal tissues *in vivo*. Although, CD22 has a rapid endocytosis rate following ligation, it is very probable that the uptake of RFB4-CNT will be substantially slower and lower than that of the targeting MAb due to the increase in size. Indeed, previously published reports indicate that the amount of internalized chimeric tetravalent RFB4 in Daudi cells after 8 hr of incubation was ~15% lower than that of a divalent RFB4 due to a 33% higher molecular weight.[48] The rate of RFB4-CNT internalization and the consequences on the efficiency of NIR mediated thermal ablation will be pursued in a future study. On the long range, it will be important to compare the *in vivo* behavior of both the noncovalent MAb-CNTs and the covalent MAb-CNTs with regard to biodistribution, PK, and toxicity. Such studies are ongoing in both normal and tumor-bearing mice.

Acknowledgements

This research was supported by the Cancer Immunobiology Center, DOD grant W81XWH-08-20004, Norman Hackerman Texas Advanced Research (Biological Sciences) Program grant No. 009741-0005-2007 and the Robert A. Welch Foundation (P.P.; grant AT-1364 and I.H.M.; grant AT-1326). We thank Dr. Winston Layne (UT Dallas) for assistance with Raman spectroscopy and Ms. Linda Berry (UT Southwestern) for assistance with the manuscript.

References

1. Weissleder R. A clearer vision for *in vivo* imaging. Nat Biotechnol 2001;19:316–17.
2. Kam NWS, O'Connell M, Wisdom JA, Dai H. Carbon nanotubes as multifunctional biological transporters and near-infrared agents for selective cancer cell destruction. Proc Natl Acad Sci USA 2005;102:11600–5.
3. Liu Z, Cai W, He L, Nakayama N, Chen K, Sun X, Chen X, Dai H. In vivo biodistribution and highly efficient tumor targeting of carbon nanotubes in mice. Nat Nanotechnol 2007;2:47–52.
4. Gobin AM, Lee MH, Halas NJ, James WD, Drezek RA, West JL. Near-infrared resonant nanoshells for combined optical imaging and photothermal cancer therapy. Nano Lett 2007;7:1929–34.
5. Loo C, Lowery A, Halas N, West J, Drezek R. Immunotargeted nanoshells for integrated cancer imaging and therapy. Nano Lett 2005;5:709–11.
6. Huang X, El-Sayed IH, Qian W, El-Sayed MA. Cancer cell imaging and photothermal therapy in the near-infrared region by using gold nanorods. J Am Chem Soc 2006;128:2115–20.
7. Hirsch LR, Stafford RJ, Bankson JA, Sershen SR, Rivera B, Price RE, Hazle JD, Halas NJ, West JL. Nanoshell-mediated near-infrared thermal therapy of tumors under magnetic resonance guidance. Proc Natl Acad Sci USA 2003;100:13549–54.
8. Shao N, Lu S, Wickstrom E, Panchapakesan B Integrated molecular targeting of IGF1R and Her2 surface receptors and destruction of breast cancer cells using single wall carbon nanotubes. Nanotechnology 2007;18:315101–9.
9. Falk MH, Issels RD. Hyperthermia in oncology. Int J Hyperthermia 2001;17:1–18.
10. Wust P, Hildebrandt B, Sreenivasa G, Rau B, Gellermann J, Riess H, Felix R, Schlag PM. Hyperthermia in combined treatment of cancer. Lancet Oncol 2002;3:487–97.
11. Singh R, Pantarotto D, Lacerda L, Pastorin G, Klumpp C, Prato M, Bianco A, Kostarelos K. Tissue biodistribution and blood clearance rates of intravenously administered carbon nanotube radiotracers. Proc Natl Acad Sci USA 2006;103:3357–62.

12. Cherukuri P, Gannon CJ, Leeuw TK, Schmidt HK, Smalley RE, Curley SA, Weisman RB. Mammalian pharmacokinetics of carbon nanotubes using intrinsic near-infrared fluorescence. Proc Natl Acad Sci USA 2006;103:18882–6.
13. Liu Z, Davis C, Cai W, He L, Chen X, Dai H. Circulation and long-term fate of functionalized, biocompatible single-walled carbon nanotubes in mice probed by Raman spectroscopy. Proc Natl Acad Sci USA 2008;105:1410–5.
14. McDevitt MR, Chattopadhyay D, Kappel BJ, Jaggi JS, Schiffman SR, Antczak C, Njardarson JT, Brentjens R, Scheinberg DA. Tumor targeting with antibody-functionalized, radiolabeled carbon nanotubes. J Nucl Med 2007;48:1180–9.
15. Liu Z, Sun X, Nakayama-Ratchford N, Dai H. Supramolecular chemistry on water-soluble carbon nanotubes for drug loading and delivery. ACS Nano 2007;1:50–6.
16. Welsher K, Liu Z, Daranciang D, Dai H. Selective probing and imaging of cells with single walled carbon nanotubes as near-infrared fluorescent molecules. Nano Lett 2008;8:586–90.
17. Chakravarty P, Marches R, Zimmerman NS, Swafford AD, Bajaj P, Musselman IH, Pantano P, Draper RK, Vitetta ES. Thermal ablation of tumor cells with antibody-functionalized single-walled carbon nanotubes. Proc Natl Acad Sci USA 2008;105:8697–702.
18. Coleman KS, Azamian BR, Davis JJ, Bagshaw CB, Green MLH. Chemistry, biochemistry, and electrochemistry of single-walled carbon nanotubes. Pap Am Chem 2002;S224:U420–1.
19. Bianco A, Kostarelos K, Partidos CD, Prato M. Biomedical applications of functionalized carbon nanotubes. Chem Commun 2005;571–7.
20. Lin Y, Taylor S, Li HP, Fernando KAS, Qu LW, Wang W, Gu LR, Zhou B, Sun YP. Advances toward bioapplications of carbon nanotubes. J Mater Chem 2004;14:527–41.
21. Huang W, Taylor S, Fu K, Lin Y, Zhang D, Hanks TW, Rao AM, Sun Y. Attaching proteins to carbon nanotubes via diimide-activated amidation. Nano Lett 2002;2:311–4.
22. Itkis ME, Perea DE, Niyogi S, Rickard SM, Hamon MA, Hu H, Zhao B, Haddon RC. Purity evaluation of as-prepared single-walled carbon nanotube soot by use of solution-phase near-IR spectroscopy. Nano Lett 2003;3:309–14.
23. Lauret JS, Voisin C, Cassabois G, Delalande C, Roussignol P, Jost O, Capes L Ultrafast carrier dynamics in single wall carbon nanotubes. Phys Rev Lett 2003;90:057404.
24. Zuckier LS, Rodriguez LD, Scharff MD. Immunologic and pharmacologic concepts of monoclonal antibodies. Semin Nucl Med 1989;29:166–86.
25. Ghetie V, Thorpe P, Ghetie MA, Knowles P, Uhr JW, Vitetta ES. The GLP large scale preparation of immunotoxins containing deglycosylated ricin A chain and a hindered disulfide bond. J Immunol Methods 1991;142:223–30.
26. Engert A, Martin G, Amlot P, Wijdenes J, Diehl V, Thorpe P. Immunotoxins constructed with anti-CD25 monoclonal antibodies and deglycosylated ricin A-chain have potent anti-tumour effects against human Hodgkin cells in vitro and solid Hodgkin tumours in mice. Int J Cancer 1991;49:450–6.
27. Poenitzsch VZ, Musselman IH. Atomic force microscopy measurements of peptide-wrapped single-walled carbon nanotube diameters. Microsc Microanal 2006;12:221–7.
28. Yehia H, Draper RK, Mikoryak C, Walker E, Bajaj P, Musselman I, Daigrepont M, Dieckmann G, Pantano P. Single-walled carbon nanotube interactions with HeLa cells. J Nanobiotechnol 2007;5:8–24.
29. Wang Y, Iqbal Z, Mitra S. Rapidly functionalized, water-dispersed carbon nanotubes at high concentration. J Am Chem Soc 2006;128: 95–9.
30. Bottini M, Bruckner S, Nika K, Bottini N, Bellucci S, Magrini A, Bergamaschi A, Mustelin T. Multi-walled carbon nanotubes induce T lymphocyte apoptosis. Toxicol Lett 2006;160:121–6.
31. Magrez A, Kasas S, Salicio V, Pasquier N, Seo JW, Celio M, Catsicas S, Schwaller B, Forro L. Cellular toxicity of carbon-based nanomaterials. Nano Lett 2006;6:1121–5.
32. Dumortier H, Lacotte S, Pastorin G, Marega R, Wu W, Bonifazi D, Briand JP, Prato M, Muller S, Bianco. Functionalized carbon nanotubes are non-cytotoxic and preserve the functionality of primary immune cells. Nano Lett 2006;6:1522–8.
33. Schipper ML, Nakayama-Ratchford N, Davis CR, Kam NW, Chu P, Liu Z, Sun X, Dai H, Gambhir SS. A pilot toxicology study of single-walled carbon nanotubes in a small sample of mice. Nat Nanotechnol 2008;3:216–21.
34. Sayes CM, Liang F, Hudson JL, Mendez J, Guo W, Beach JM, Moore VC, Doyle CD, West JL, Billups WE, Ausman KD, Colvin VL. Functionalization density dependence of single-walled carbon nanotubes cytotoxicity *in vitro*. Toxicol Lett 2006;161:135–42.
35. Ghetie MA, Picker LJ, Richardson JA, Tucker K, Uhr JW, Vitetta ES. Anti-CD19 inhibits the growth of human B-cell tumor lines in vitro and of Daudi cells in SCID mice by inducing cell cycle arrest. Blood 1994;83:1329–36.
36. Marches R, Scheuermann RH, Uhr JW. Cancer dormancy: role of cyclin-dependent kinase inhibitors in induction of cell cycle arrest mediated via membrane IgM. Cancer Res 1998;58:691–7.
37. Cherukuri P, Bachilo SM, Litovsky SH, Weisman RB. Near-infrared fluorescence microscopy of single-walled carbon nanotubes in phagocytic cells. J Am Chem Soc 2004;126:15638–9.
38. Kam NWS, Jessop TC, Wender PA, Dai H. Nanotube molecular transporters: internalization of carbon nanotube-protein conjugates into mammalian cells. J Am Chem Soc 2004;126:6850–1.
39. Pantarotto D, Briand J-P, Prato M, Bianco A. Translocation of bioactive peptides across cell membranes by carbon nanotubes. Chem Commun (*Camb*) 2004;1:16–7.
40. Lu Q, Moore JM, Huang G, Mount AS, Rao AM, Larcom LL, Ke PC. RNA polymer translocation with single-walled carbon nanotubes. Nano Lett 2004;4:2473–7.
41. Bianco A, Hoebeke J, Godefroy S, Chaloin O, Pantarotto D, Briand JP, Muller S, Prato M, Partidos CD. Cationic carbon nanotubes bind to CpG oligodeoxynucleotides and enhance their immunostimulatory properties. J Am Chem Soc 2005;127:58–9.
42. Kostarelos K, Lacerda L, Pastorin G, Wu W, Wieckowski S, Luangsivilay J, Godefroy S, Pantarotto D, Briand JP, Muller S, Prato M, Bianco A. Cellular uptake of functionalized carbon nanotubes is independent of functional group and cell type. Nat Nanotechnol 2006;2:108–13.
43. Ghetie MA, May RD, Till M, Uhr JW, Ghetie V, Knowles PP, Relf M, Brown A, Wallace PM, Janossy G, Amlot P, Vitetta ES, Thorpe PE. Evaluation of ricin A chain-containing immunotoxins directed against CD19 and CD22 antigens on normal and malignant human B-cells as potential reagents for in vivo therapy. Cancer Res 1988;48:2610–7.
44. Vitetta ES, Stone M, Amlot P, Fay J, May R, Till M, Newman J, Clark P, Collins R, Cunningham D. Phase I immunotoxin trial in patients with B-cell lymphoma. Cancer Res 1991;51:4052–8.
45. Press OW, Farr AG, Borroz KI, Anderson SK, Martin PJ. Endocytosis and degradation of monoclonal antibodies targeting human B-cell malignancies. Cancer Res 1989;49:4906–12.
46. Amlot PL, Stone MJ, Cunningham D, Fay J, Newman J, Collins R, May R, McCarthy M, Richardson J, Ghetie V, Ramilo O, Thorpe PE, et al. A phase I study of an anti-CD22-deglycosylated ricin A chain immunotoxin in the treatment of B-cell lymphomas resistant to conventional therapy. Blood 1993;82:2624–33.
47. Shan D, Press OW. Constitutive endocytosis and degradation of CD22 by human B cells. J Immunol 1995;154:4466–75.
48. Liu X, Pop LM, Roopenian DC, Ghetie V, Vitetta ES, Smallshaw JE. Generation and characterization of a novel tetravalent anti-CD22 antibody with improved antitumor activity and pharmacokinetics. Int Immunopharmacol 2006;6:791–9.